Effector membrane translocation biosensors reveal G protein and βarrestin coupling profiles of 100 therapeutically relevant GPCRs

Charlotte Avet[1†], Arturo Mancini[2†], Billy Breton[2‡§], Christian Le Gouill[1‡], Alexander S. Hauser[3‡], Claire Normand[2], Hiroyuki Kobayashi[1], Florence Gross[2], Mireille Hogue[1], Viktoriya Lukasheva[1], Stéphane St-Onge[1], Marilyn Carrier[1], Madeleine Héroux[1], Sandra Morissette[2], Eric Fauman[4], Jean-Philippe Fortin[5], Stephan Schann[6], Xavier Leroy[6*], David E. Gloriam[3*], and Michel Bouvier[1*].

[1]Institute for Research in Immunology and Cancer (IRIC), and Department of Biochemistry and Molecular Medicine, Université de Montréal; Montréal, Québec, H3T 1J4, Canada.
[2]Domain Therapeutics North America; Montréal, Québec, H4S 1Z9, Canada.
[3]Department of Drug Design and Pharmacology; University of Copenhagen; 2100 Copenhagen, Denmark.
[4]Internal Medicine Research Unit; Pfizer Worldwide Research, Development and Medical; Cambridge, MA 02139, USA.
[5]Pfizer Global R&D; Cambridge, MA 02139, USA.
[6]Domain Therapeutics; 67400 Illkirch-Strasbourg, France.
[†]These authors contributed equally.
[‡]These authors contributed equally.
[§]Current address: Institute for Research in Immunology and Cancer (IRIC), Université de Montréal; Montréal, Québec, H3T 1J4, Canada.

*** Corresponding authors**:

Michel Bouvier ; IRIC, Université de Montréal : michel.bouvier@umontreal.ca,

David E. Gloriam; University of Copenhagen: david.gloriam@sund.ku.dk,

Xavier Leroy; Domain Therapeutics: xleroy@domaintherapeutics.com

Abstract

The recognition that individual GPCRs can activate multiple signaling pathways has raised the possibility of developing drugs selectively targeting therapeutically relevant ones. This requires tools to determine which G proteins and βarrestins are activated by a given receptor. Here, we present a set of BRET sensors monitoring the activation of the 12 G protein subtypes based on the translocation of their effectors to the plasma membrane (EMTA). Unlike most of the existing detection systems, EMTA does not require modification of receptors or G proteins (except for G_s). EMTA was found to be suitable for the detection of constitutive activity, inverse agonism, biased signaling and polypharmacology. Profiling of 100 therapeutically relevant human GPCRs resulted in 1,500 pathway-specific concentration-response curves and revealed a great diversity of coupling profiles ranging from exquisite selectivity to broad promiscuity. Overall, this work describes unique resources for studying the complexities underlying GPCR signaling and pharmacology.

Introduction

G protein-coupled receptors (GPCRs) play crucial roles in the regulation of a wide variety of physiological processes and represent one-third of clinically prescribed drugs (Hauser, Attwood, Rask-Andersen, Schioth, & Gloriam, 2017). Classically, GPCR-mediated signal transduction was believed to rely on linear signaling pathways whereby a given GPCR selectively activates a single G protein family, defined by the nature of its Gα subunit (Oldham & Hamm, 2008). Gα proteins are divided into four major families (G_s, $G_{i/o}$, $G_{q/11}$, and $G_{12/13}$) encoded by 16 human genes. Once activated, these proteins each trigger different downstream effectors yielding different biological outcomes. It has now become evident that many GPCRs can couple to more than one G protein family and that ligands can selectively promote the activation of different subsets of these pathways (Namkung et al., 2018; Quoyer et al., 2013). These observations extended the concept of ligand-biased signaling, which was first established for ligand-directed selectivity between βarrestin and G protein (Azzi et al., 2003; Wei et al., 2003), to functional selectivity between G proteins. Ligand-directed functional selectivity represents a promising avenue for GPCRs drug discovery since it offers the opportunity of activating pathways important for therapeutic efficacy while minimizing activation of pathways responsible for undesirable side effects (Galandrin, Oligny-Longpre, & Bouvier, 2007; Kenakin, 2019).

To fully explore the potential of functional selectivity, it is essential to have an exhaustive description of the signaling partners that can be activated by a given receptor, providing receptor- and ligand-specific signaling signatures. Currently, few assays allow for an

exhaustive pathway-specific analysis of GPCR signaling; these include BRET-based G protein activation sensors platforms (Gales et al., 2005; Masuho et al., 2015; Maziarz et al., 2020; Mende et al., 2018; Olsen et al., 2020) and the TGF-α shedding assay (Inoue et al., 2019). However, several of these platforms require modification of G protein subunits that may create functional distortions. Moreover, these assays may detect non-productive conformational rearrangements of the G protein heterotrimer as was recently reported for G_{12} (Okashah et al., 2020).

Here, we describe unique sensors that do not require modification of receptors or G proteins (except for G_s) for interrogating the signaling profiles of GPCRs. The platform includes 15 pathway-selective enhanced bystander bioluminescence resonance energy transfer (ebBRET) biosensors monitoring the translocation of downstream effectors to the plasma membrane for $G_{i/o}$, $G_{q/11}$ and $G_{12/13}$, the dissociation of the Gα subunit from the plasma membrane for G_s and the recruitment of βarrestin to the plasma membrane. Overall, the new ebBRET-based **E**ffector **M**embrane **T**ranslocation **A**ssays, named EMTA, provide a readily accessible large scale and comprehensive platform to study constitutive and ligand-directed GPCR signaling. The signaling signatures of 100 GPCRs using the EMTA platform also provides a rich source of information to explore the principles underlying receptor/G protein/βarrestin coupling selectivity relationships. It thus provides a unique set of tools that is complementary to previously described platforms and existing datasets, and offers a map of the coupling potentials for individual GPCR that will

stimulate future studies investigating the relevance of these couplings in different physiological systems.

Results

ebBRET-based G protein effector membrane translocation assay (EMTA) allows detection of each Gα protein subunit activation

To detect the activation of Gα subtypes, we created an EMTA biosensor platform based on ebBRET (Namkung et al., 2016) (**Figure 1A**). The biosensors at the heart of EMTA consist of sub-domains of the G protein-effector proteins p63-RhoGEF, Rap1GAP and PDZ-RhoGEF that selectively interact with activated $G_{q/11}$, $G_{i/o}$ or $G_{12/13}$, respectively. These domains were fused at their C-terminus to *Renilla* luciferase (RlucII) and co-expressed with different unmodified receptor and Gα protein subtypes. Upon GPCR activation, the energy donor-fused effectors translocate to the plasma membrane to bind activated Gα proteins, bringing RlucII in close proximity to the energy acceptor, *Renilla* green fluorescent protein, targeted to the plasma membrane through a CAAX motif (rGFP-CAAX), thus leading to an increase in ebBRET. The same plasma membrane translocation principle is used to measure βarrestin recruitment (Namkung et al., 2016) (**Figure 1B,** top). Because no selective soluble downstream effector of G_s exists, the assay was modified taking advantage of $G\alpha_s$ dissociation from the plasma membrane following its activation (Wedegaertner, Bourne, & von Zastrow, 1996). In this configuration, the RlucII is directly fused to $G\alpha_s$ (Carr et al., 2014). Its activation upon GPCR stimulation leads to its dissociation from the plasma membrane (Martin & Lambert, 2016), resulting in a reduction in ebBRET (**Figure 1B,** bottom).

The sensitivity and selectivity of the newly created G protein EMTA biosensors, were validated using prototypical GPCRs known to activate specific Gα subtypes. The responses were monitored upon heterologous expression of specific Gα subunits belonging to $G_{i/o}$, $G_{q/11}$ or $G_{12/13}$ families in the absence or presence of pharmacological inhibitors and using engineered cells lacking selected Gα subtypes. The dopamine D_2 receptor was used to validate the ability of the $G_{i/o}$ binding domain of Rap1GAP (Jordan, Carey, Stork, & Iyengar, 1999; Meng, Glick, Polakis, & Casey, 1999) to selectively detect $G_{i/o}$ activation. The dopamine-promoted increase in ebBRET between Rap1GAP-RlucII and rGFP-CAAX in the presence of $G\alpha_{i/o}$ subunits was not affected by the $G_{q/11}$-selective inhibitor UBO-QIC (a.k.a., FR900359 (Schrage et al., 2015); **Figure 2A**, left), whereas the $G\alpha_{i/o}$ family inhibitor, pertussis toxin (PTX), completely blocked the response for all members of $G\alpha_{i/o}$ family except for $G\alpha_z$, known to be insensitive to PTX (Casey, Fong, Simon, & Gilman, 1990) (**Figure 2A**, right). Gonadotropin-releasing hormone (GnRH) stimulation of the GnRH receptor (GnRHR), used as a prototypical $G_{q/11}$-coupled receptor, promoted ebBRET between the RlucII-fused $G_{q/11}$ binding domain of p63-RhoGEF (p63-RhoGEF-RlucII) (Lutz et al., 2007; Rojas et al., 2007) and rGFP-CAAX. The ebBRET increase observed in the presence of different $G\alpha_{q/11}$ subunits was not significantly ($p=0.077$, 0.0636 and 0.073 for G_q, G_{11} and G_{14}, respectively) affected by PTX (**Figure 2B**, right), whereas UBO-QIC completely blocked the response for all members of $G\alpha_{q/11}$ family except for $G\alpha_{15}$, known to be insensitive to UBO-QIC (Schrage et al., 2015) (**Figure 2B**, left). These two G protein specific EMTA were sensitive enough to detect responses elicited by endogenous G proteins since deletion of $G_{i/o}$ ($\Delta G_{i/o}$) or $G_{q/11}$ ($\Delta G_{q/11}$) subtypes completely abolished the

responses induced by D_2 or GnRHR activation in the absence of heterologously expressed G proteins (**Figure S1I**). It should however be noted that relying on endogenous proteins does not allow the identification of specific members of $G_{i/o}$ (i.e.: G_{i1}, G_{i2}, G_{i3}, G_{oA}, G_{oB} or G_z) or $G_{q/11}$ (i.e.: G_q, G_{11}, G_{14} or G_{15}) families.

The selectivity of the $G_{12/13}$ binding domain of PDZ-RhoGEF (Fukuhara, Chikumi, & Gutkind, 2001) was confirmed using the cannabinoid receptor type 1 (CB_1). The ebBRET between PDZ-RhoGEF-RlucII and rGFP-CAAX in the presence of $G\alpha_{12}$ or $G\alpha_{13}$ promoted by the cannabinoid agonist WIN-55,212-2 was not affected by UBO-QIC (**Figure 2C**, top left), nor PTX (**Figure 2C**, top right). Given the lack of selective $G_{12/13}$ pharmacological inhibitor, we used HEK293 cells genetically deleted for $G\alpha_{12}$ and $G\alpha_{13}$ proteins ($\Delta G_{12/13}$) to further confirm the response selectivity. As expected, PDZ-RhoGEF-RlucII/rGFP-CAAX ebBRET was observed only following reintroduction of either $G\alpha_{12}$ ($\Delta G_{12/13}$_+G_{12}) or $G\alpha_{13}$ ($\Delta G_{12/13}$_+G_{13}) (**Figure 2C**, bottom left). The $G_{12/13}$ coupling of CB_1 was further confirmed by monitoring the recruitment of PKN to the plasma membrane (**Figure 2C**, bottom right) in agreement with previous reports (Inoue et al., 2019).

To further assess the selectivity of each EMTA biosensor, we took advantage of the fact that the endothelin-1 receptor (ET_A) can activate $G_{q/11}$, $G_{i/o}$ and $G_{12/13}$ family members. As shown in **Figure S2,** only over-expression of the Gα family members corresponding to their selective effectors (Rap1GAP for $G_{i/o}$, p63-RhoGEF for $G_{q/11}$ and PDZ-RhoGEF for $G_{12/13}$) significantly increased the recruitment of the effector-RlucII to the plasma

membrane. A recent study (Chandan N.R., 2021) showed that $G_{i/o}$ can also activate full length PDZ-RhoGEF. Although the domain of PDZ-RhoGEF required for this activation has not been identified yet, the selectivity of our PDZ-RhoGEF sensor for $G_{12/13}$ *vs.* all other G protein families most likely results from the fact that we used a truncated version of PDZ-RhoGEF that only contains the $G_{12/13}$ binding domain and lacks the PDZ domain involved in protein-protein interaction, the actin-binding domain and the DH/PH domains involved in GEF activity and RhoA activation (Aittaleb, Boguth, & Tesmer, 2010).

It should be noted that in the heterologous expression configuration, competition with endogenous G proteins did not occur to a significant extent since the potencies of the responses to a given G protein subtype were not affected by genetic deletion of the different G protein family members (**Figure S1** and **Supplementary Table 1A**). Similarly, overexpression of G proteins, GPCRs or effectors-RlucII did not affect the potencies of the responses observed (**Figure S3** and **Supplementary Table 1B-D**), indicating that, in our experimental conditions, overexpression of the different components of EMTA sensors must likely not bias the coupling response. In addition to spectrometric assessment of coupling selectivity (above) and activation kinetics (**Figure S4**), EMTA allows to image the real-time recruitment of the G protein effectors to the plasma membrane (**Videos 1-3**) thus providing spatiotemporal resolution for the imaging detection of $G\alpha_{i/o}$, $G\alpha_{q/11,14,15}$ and $G\alpha_{12/13}$ activation.

The sensitivity of the EMTA platform is illustrated by a direct side-by-side comparison of the signals detected with EMTA *vs.* BRET assays based on Gαβγ dissociation (Gαβγ) (Gales

et al., 2005; Gales et al., 2006; Olsen et al., 2020), that reveals a significantly larger assay windows for EMTA for the 6 Gα subunits tested for 8 selected receptors, (**Figure S5**).

For the $G\alpha_s$ translocation biosensor, the bile acid receptor (GPBA) was chosen for validation (Kawamata et al., 2003). As expected, lithocholic acid stimulation resulted in a concentration-dependent decrease in ebBRET between $G\alpha_s$-RlucII and rGFP-CAAX (**Figure 2D**, left). Cholera toxin (CTX), which directly activates $G\alpha_s$ (De Haan & Hirst, 2004), led to a decrease in ebBRET (**Figure 2D**, center), confirming that loss of $G\alpha_s$ plasma membrane localization results from its activation. The potency of lithocholic acid to promote G_s dissociation from the plasma membrane was well in line with its potency to increase cAMP production as assessed using a BRET²-based EPAC biosensor (Leduc et al., 2009) (**Figure 2D**, right). The G_s-plasma membrane dissociation ebBRET signal was not affected by UBO-QIC or PTX (**Figure 2D**, left), confirming the selectivity of the biosensor.

Signaling signatures of one hundred therapeutically relevant receptors reveals distinct G protein and βarrestin selectivity profiles

We used EMTA to assess the signaling signature of a panel of 100 human GPCRs that are either already the target of clinically used drugs (74 receptors), considered for pre- or clinical drug development (6 receptors), or pathophysiologically relevant (**Supplementary Table S2A**). To establish the coupling potentials for each receptor, we quantified its ability to activate 15 pathways: $G\alpha_s$, $G\alpha_{i1}$, $G\alpha_{i2}$, $G\alpha_{oA}$, $G\alpha_{oB}$, $G\alpha_z$, $G\alpha_{12}$, $G\alpha_{13}$, $G\alpha_q$, $G\alpha_{11}$, $G\alpha_{14}$, $G\alpha_{15}$ and βarrestin 2 as well as βarrestin 1 and 2 in presence of GRK2 (**Supplementary File 1**).

196 E_{max} and pEC_{50} values were determined (**Supplementary Table 2**) and, based on the pre-
197 determined threshold criteria (Emax ≥ mean of vehicle-stimulated + 2*SD; see Methods),
198 a 'yes or no' agonist-dependent activation was assigned to each signaling pathway and
199 summarized using radial graph representations (**Figure S7**). To assess whether
200 endogenous receptors could contribute to the observed responses, assays were also
201 carried out in cells not transfected with the studied receptor (**Figure S8**). When an
202 agonist-promoted response was observed in non-transfected parental HEK293 cells, this
203 response was not considered as a receptor-specific response (see Methods).
204
205 To compare the signaling profiles across all receptors and pathways and to overcome
206 differences in receptor expression levels and individual biosensor dynamic windows, we
207 first min-max normalized E_{max} and pEC_{50} values (between 0 and 1) across receptors as a
208 function of a reference receptor yielding the largest response for a given pathway (**Figure**
209 **3A**, left). Then, these values were again min-max normalized (between 0 and 1) for the
210 same receptor across pathways, using the pathway with the largest response for this
211 receptor as the reference (**Figure 3A**, right; see description in Methods). Such double
212 normalization allows direct comparison of the coupling efficiency to different G proteins
213 for a given receptor and across receptors for a given G protein. This coupling efficiency is
214 summarized as heatmaps (**Figure 3B**) that reveals a high diversity of signaling profiles. The
215 selectivity toward the different G protein families varies considerably among GPCRs
216 (**Figure 4**). In our dataset, which is the first using unmodified GPCRs and Gα proteins
217 (except for G_s), 29% of the receptors coupled to only one family, whereas others displayed

more promiscuity by coupling to 2, 3 or 4 families (36%, 25% and 10% respectively). Receptors coupling to a single G protein family favored the members of the $G_{i/o}$ family. Indeed, 27% of the receptors coupling to $G_{i/o}$ only activated this subtype family in comparison to 0, 2.4 and 9.1% for receptors activating $G_{12/13}$, $G_{q/11}$ and G_s, respectively, thus displaying more promiscuous coupling. A detailed comparative analysis of the selectivity profiles that we observed using the EMTA sensors with that of the chimeric G protein-based assay developed by Inoue *et al.* (Inoue et al., 2019) and the IUPHAR/BPS Guide to Pharmacology database (GtP; https://www.guidetopharmacology.org/) is presented in the accompanying paper (Hauser et al., 2021). **Supplementary Table 2C** allows a direct comparison of the relative potency determined using EMTA for both the new and the already known (i.e.: identified in GtP database) couplings. As can be seen in the table, although in many cases the potency for the novel couplings is lower, this is not a universal finding since for some receptors, the pEC_{50}s for the new couplings are similar (ex: G_{12} for CB_1; G_{13} for serotonin 5-HT_{2C}; $G_{12/13}$ for adenosine 2A (A_{2A}) and prostaglandin E1 (EP_1) receptors; $G_{i/o}$ for corticotropin-releasing hormone receptor 1 (CRFR1), ET_A and G-protein-coupled receptor 39 (GPR39)) or higher (ex: G_z for serotonin 5-HT_{2B}; G_{15} for adenosine 3 (A_3) and melanocortin 3 (MC3R) receptors; G_{12} for bradykinin 2 (B_2), cholecystokinin A (CCK_1), chemokine receptor 6 (CCR6) and ET_A receptors; $G_{12/13}$ for CRFR1 and GPR68) than those for the canonical ones. Interestingly, in many instances the potency for the newly uncovered couplings are similar to those for βarrestins, which is generally lower than for their canonical G proteins, a finding consistent with the role of βarrestins in signaling arrest at the plasma membrane. The potency differences observed

for the activation of different G protein subtypes by a given receptor may lead to preferential activation of some pathways over others. This relative selectivity is likely to be influenced by tissue-dependent G protein subtype expression levels. The physiological consequences of such selectivity remain to be investigated.

When examining the frequency of coupling for each Gα subunit family (**Figure 4C**), the $G_{i/o}$ family members were the most commonly activated, with 89% of the tested receptors activating a $G_{i/o}$ family member. In contrast, only 33%, 49% and 45% of the receptors activate G_{s}, $G_{12/13}$ or $G_{q/11}$ (excluding $G\alpha_{15}$) family members, respectively. Not surprisingly, and consistent with its reported promiscuous coupling, $G\alpha_{15}$ was found to be activated by 81% of the receptors. For some receptors, we also observed preferential coupling of distinct members within a subtype family (**Figure S7**). For instance, 33% of $G_{i/o}$-coupled receptors can couple to only a subpopulation of the family (**Figure S10A**). For the $G_{q/11}$ family, only 44% activate all family members with 45% activating only $G\alpha_{15}$ and 11% engaging only 2 or 3 members of the family. A matrix expressing the % of receptors engaging a specific Gα subtype that also activated another subtype, is illustrated in **Figure S10B.** When considering individual families, considerable variation within the $G_{i/o}$ family was observed. The greatest similarities were observed between $G\alpha_{oB}$ and either $G\alpha_{oA}$ or $G\alpha_{z}$, and the lowest between $G\alpha_{i1}$ and $G\alpha_{z}$. A striking example of intra-family coupling selectivity is the serotonin 5-HT_{2B} that activates only $G\alpha_{oB}$ and $G\alpha_{z}$ and GPR65 that selectively activates $G\alpha_{oB}$. Similarly, when considering the ligand-promoted responses above our threshold criteria (see Methods), histamine H_2 and MC3R receptors show

preferred activation of $G\alpha_{oB}$ and $G\alpha_{z}$, whereas the prostaglandin F (FP) and neuropeptide Y5 (Y_5) receptors preferentially activate $G\alpha_{oB}$, $G\alpha_{oA}$ and $G\alpha_{z}$. Even when all members of a given family are found to be activated, some receptors activate specific family members with greater potencies (**Supplementary Table 2C**).

When considering βarrestin recruitment, our analysis shows that 22% of receptors did not recruit βarrestin1 or 2, even in the presence of overexpressed GRK2 (**Figure 4D**). Among the receptors able to recruit βarrestins, only a very small number selectively recruited βarrestin1 (1.3%) or βarrestin2 (6.4%), most of them recruiting both βarrestins in the presence of GRK2 (92.3%) (**Figure 4D**). Overexpression of GRK2 potentiated the recruitment of βarrestin2 for 68% of receptors highlighting the importance of GRK2 expression level in determining βarrestin activation (**Supplementary File 1** and **Supplementary Table 2**).

Comparison with Previous Datasets Reveals Commonalities and Crucial Differences

We compared the signaling profiles obtained here with those presented by Inoue *et al.* (Inoue et al., 2019) and the GtP dataset. Of note, this comparison only considers the final reported couplings that in the Inoue's study were based on the criteria of positive coupling if LogRAi ≥ -1 and negative coupling if LogRAi ≤ -1, and is influenced by the different cut-offs and normalization used in the two studies. A comparison of couplings using common Emax standard deviation cut-off, quantitative normalization and aggregation of G proteins into families is provided in the accompanying paper (Hauser et

al., 2021). As can be seen in **Supplementary Table 3A**, among the 70 receptors common to both studies, less couplings were detected in our study than reported in Inoue *et al.* for $G\alpha_s$ (21 *vs.* 28), $G\alpha_{i1}$ (54 *vs.* 56), $G\alpha_q$ (31 *vs.* 34) and $G\alpha_{14}$ (36 *vs.* 40). In contrast, more receptors activating $G\alpha_{12}$ (29 *vs.* 23), $G\alpha_o$ (59 *vs.* 41), $G\alpha_{13}$ (30 *vs.* 15), $G\alpha_z$ (52 *vs.* 37) and $G\alpha_{15}$ (62 *vs.* 15) were detected in our study. When comparing with data collected in GtP, that reports couplings grouped for G protein families (*i.e.*: G_s, $G_{i/o}$, $G_{q/11}$ or $G_{12/13}$) and not at the single G protein subtype level, we detected less couplings than what was reported in GtP for $G\alpha_s$ (32 *vs.* 37), but more for $G\alpha_{i/o}$ (89 *vs.* 69), $G\alpha_{q/11}$ (81 *vs.* 48) and $G\alpha_{12/13}$ (47 *vs.* 10), among the 99 receptors common to both datasets (**Supplementary Table 3B**).

Altogether, the comparative analysis reveals 64% and 69% identity of couplings between the EMTA and Inoue's or GtP datasets, respectively. Each dataset reporting unique couplings and missing couplings found in the other two datasets. The reasons for these differences are plausibly due to intrinsic differences in the assays used. For instance, for $G_{12/13}$ and G_{15} specifically, the difference with the GtP dataset most likely results from the fact that in most cases $G_{12/13}$ or G_{15} activation were determined indirectly since, until their recent description ($G_{12/13}$: (Quoyer et al., 2013; Schrage et al., 2015); G_{15}:(Inoue et al., 2019; Olsen et al., 2020)), no robust readily available assay existed to monitor the activation of these G proteins.

Validation of newly identified $G_{12/13}$ and G_{15} couplings

Given the overrepresentation of both $G_{12/13}$ and G_{15} couplings, obtained with the EMTA assays *vs.* those reported by Inoue *et al.* and the GtP datasets, the validity of the EMTA assay to detect real productive couplings, was confirmed using orthogonal assays for selective examples not reported in the two other datasets. For $G_{12/13}$, we used the PKN-based BRET biosensor detecting Rho activation downstream of either $G_{12/13}$ or $G_{q/11}$ (Namkung et al., 2018) and the MyrPB-Ezrin-based BRET biosensor detecting the activation of Ezrin downstream of $G_{12/13}$ (Leguay et al., 2021), both in the absence of heterologously expressed G proteins. Ligand stimulation of FP and $CysLT_2$ receptors led to Rho and ezrin activation (**Figure S9A**), that were insensitive to the $G_{q/11}$ inhibitor YM-254890, confirming that these receptors activate $G\alpha_{12/13}$.

For newly identified G_{15} couplings we took advantage of the lack of $G\alpha_{15}$ in HEK293 cells and assessed the impact of $G\alpha_{15}$ heterologous expression on receptor-mediated calcium responses (**Figure S9B**). For prostaglandin E2 (EP_2) and κ-opioid (κOR) receptors, which couple to G_{15} but no other $G_{q/11}$ members, expression of $G\alpha_{15}$ significantly increased the PGE2- and Dynorphin A- promoted calcium responses. For α_{2A} adrenergic (α_{2A}AR) and vasopressin 2 (V_2) receptors that couple other $G_{q/11}$ family members, treatment with YM-254890 completely abolished the agonist-promoted calcium response in the absence of $G\alpha_{15}$. In contrast, the calcium response evoked by α_{2A}AR and V_2 agonists following $G\alpha_{15}$ expression was completely insensitive to YM-254890 (**Figure S9B**), confirming that these receptors can activate this YM-254890-insensitive G protein subtype (Takasaki et al., 2004).

EMTA platform detects constitutive receptor activity and biased signaling

We went on to assess the ability of the EMTA platform to detect receptor constitutive activity. Transfection of increasing amounts of adenosine A_1 receptor (A_1) led to a receptor-dependent increase in basal ebBRET of the $G\alpha_{i2}$-activation sensor (**Figure 5A**, left), reflecting A_1 constitutive activity. The A_1 inverse agonist DPCPX (Lu et al., 2014) dose-dependently decreased the constitutive A_1-mediated activation of $G\alpha_{i2}$ (**Figure 5A**, left), indicating that EMTA can detect inverse agonism. Although we can not exclude that the high basal activity resulted from activation by adenosine in the cell culture medium, the fact that high basal activity was observed for A_1 but not A_3, despite a similar potency of adenosine to activate these two receptors subtypes (see **Figure S11A**), supports the notion that the increased basal activity reflects A_1 constitutive activity.

To further confirm that the platform can adequately detect inverse agonism, a second receptor for which no endogenous ligand should be present in the media, the CB_1 receptor, was used. As illustrated in **Figure 5A** (right), increase CB_1 expression led to a ligand-independent constitutive activation of G_z, that could be completely blocked by the CB_1 inverse agonist rimonabant.

EMTA also faithfully detected biased signaling. Indeed, as previously reported (Namkung et al., 2018; Wei et al., 2003), angiotensin analogs such as SII, saralasin or TRV027 displayed biased signaling by promoting efficient βarrestin2 recruitment but marginal or no $G\alpha_q$, $G\alpha_{i2}$ or $G\alpha_{13}$ activation as compared to angiotensin II that activated all G proteins

and βarrestin2 (**Figure 5B**). The platform was also used to identify biased-signaling resulting from single nucleotide polymorphisms. As shown in **Figure 5C**, two naturally occurring variants of human GPR17 (isoform 2) localised in the TM3 E/DRY motif resulted in altered functional selectivity profiles. Whereas the Asp128Asn variant displayed WT-like activity on $G\alpha_{i2}$, it lost the ability to activate $G\alpha_q$ and βarrestin2. In contrast, variant Arg129His at the neighboring position resulted in an increased constitutive βarrestin2 recruitment and a loss of $G\alpha_{i2}$ and $G\alpha_q$ protein signaling.

Combining G_z and G_{15} biosensors for safety panels and systems pharmacology

The G protein coupling profiles obtained for the 100 GPCRs revealed that 95% of receptors activate either $G\alpha_z$ (73%) or $G\alpha_{15}$ (81%). Measuring activation of both pathways simultaneously provides an almost universal sensor applicable to screening. Combining the two sensors (Rap1GAP-RlucII/p63-RhoGEF-RlucII/rGFP-CAAX) in the same cells allowed to detect ligand concentration-dependent activation of a safety panel of 24 GPCRs, that are well established as contributors to clinical adverse drug reactions (Bowes et al., 2012) (**Figure S12**)**.** Indeed, the G_z/G_{15} sensor captured the activation of receptors largely or uniquely coupled to either $G\alpha_z$ (e.g., CB_2) or $G\alpha_{15}$ (e.g., A_{2A} and A_{2B}), as well as receptors coupled (to varying degrees) to both pathways. The usefulness of the G_z/G_{15} combined sensor to detect off-target ligand activity is illustrated in **Figure 6A**. Most ligands tested were specific for their primary target(s). However, certain ligands displayed functional cross-reactivity with GPCRs other than their cognate targets. These included the activation of the α_{2A}AR by dopamine and serotonin, the D_2 by noradrenaline and

serotonin, and of the CB_1 and CB_2 receptors by acetylcholine (**Figures 6B-C**). The activation of D_2 by noradrenaline and serotonin was confirmed by the ability of the D_2-family selective antagonist eticlopride to block the dopamine-, serotonin- and noradrenaline-promoted responses detected using the combined G_z/G_{15} or the G_{i2}- and G_{oB}-selective sensors and βarrestin2 sensor (**Figure 6B**, top). Similarly, use of the α_2AR selective antagonist, WB4101, allowed to confirm that dopamine can activate $G\alpha_{i2}$, $G\alpha_{oB}$ and βarrestin2 through the α_{2A}AR (**Figure 6B**, bottom). Such pleiotropic activation of different monoaminergic receptors by catecholamines and serotonin has been previously observed (Roth, Sheffler, & Kroeze, 2004; Sanchez-Soto et al., 2016; Sunahara et al., 1991). Direct activation of the α_{2A}AR by dopamine was confirmed by showing that treatment with the D_2-family receptor selective antagonist eticlopride had negligible effect on dopamine-mediated activation of $G\alpha_{i2}$ and $G\alpha_{oB}$ in cells heterologously expressing α_{2A}AR, confirming that the response did not result from the activation of endogenously expressed dopamine receptor. In contrast, eticlopride blocked the activation of $G\alpha_{i2}$ and $G\alpha_{oB}$ in cells heterologously expressing D_2 (**Figure S13**).

These cross-reactivity may be direct (i.e., via direct binding of a ligand to its non-cognate receptor) as suggested above, or indirect (e.g., “trans”, via ligand activation of its canonical receptor, leading to subsequent secretion of factors that activate the non-canonical target). One such example of trans-activation is provided by the activation of cannabinoid CB_1 and CB_2 receptors by acetylcholine (detected by the $G_{z/15}$ and confirmed with the G_{oB} sensors; **Figure 6A**, **C**). Indeed, the activation was completely inhibited by

both the CB inverse agonist AM-630 and by the cholinergic antagonist atropine (**Figure 6C**, left). Yet the response evoked by the CB selective agonist WIN55,212 2 was not blocked by atropine (**Figure 6C**, center). $G\alpha_{oB}$ activation by acetylcholine did not result from direct activation of endogenous muscarinic receptors since no $G\alpha_{oB}$ response was observed in parental cells (**Figure S8**). Given that the M_3 muscarinic receptor, which is endogenously expressed at relatively high levels in HEK293 cells (Atwood, Lopez, Wager-Miller, Mackie, & Straiker, 2011), is strongly coupled to the $G_{q/11}$, CB_1-expressing cells were pretreated with $G_{q/11/14}$ inhibitor UBO-QIC prior to stimulation with acetylcholine. UBO-QIC pre-treatment blocked acetylcholine- but not WIN55,212-2-mediated $G\alpha_{oB}$ activation (**Figure 6C**, right). These results demonstrate that CB_1 activation by acetylcholine is indirect and potentially involves the secretion of an endogenous CBR ligand following activation of $G_{q/11}$ by endogenous muscarinic acetylcholine receptors. The combined G_z/G_{15} sensor is therefore a useful tool to identify interplay between receptors and to explore systems pharmacology resulting from such cross-talks.

Discussion

This study describes the development and validation of a genetically encoded ebBRET-based biosensor platform allowing live-cell mapping of GPCR-G protein coupling preferences covering 12 heterotrimeric G proteins. The novel EMTA biosensors were combined with previously described ebBRET-based βarrestin trafficking sensors (Namkung et al., 2016), providing an unprecedented description of GPCR signaling partner couplings. In addition to providing a resource to study GPCR functional selectivity (see companion paper (Hauser et al., 2021)), the sensors provide versatile and readily usable tools to study, on a large-scale, pharmacological processes such as constitutive activity, inverse agonism, ligand-biased signaling, and signaling cross-talk.

Our EMTA-based biosensor platform offers several advantages relative to other available approaches. First, EMTA provides direct real-time measurement of proximal signaling events following GPCR activation (i.e., Gα protein activation and βarrestin recruitment) and resulting in lower level of amplification than those of assays relying on enzymatic activity of downstream effectors (i.e.: adenylyl cyclase or phospholipase C) or artificial detection systems (i.e.: gene-reporter or TGF-α shedding assays) that measure signal accumulation sometimes following extended incubation times. In addition, measuring proximal activity reduces the risk of cross-talks between pathways that may complicate data interpretation when considering downstream signaling as the readout (Mancini, Frauli, & Breton, 2015).

Second, EMTA uses native untagged GPCRs and G protein subunits (except for G_s), contrary to protein complementation (Laschet, Dupuis, & Hanson, 2019), FRET/BRET-based Gαβγ dissociation/receptor-G protein interaction (Bunemann, Frank, & Lohse, 2003; Gales et al., 2005; Gales et al., 2006; Hoffmann et al., 2005; Namkung et al., 2018; Olsen et al., 2020) or TGF-α shedding (Inoue et al., 2019) assays. Modifying these core-signaling components could alter responses, complicate interpretation and explain some of the discrepancies observed between the EMTA platform and other approaches used to study G protein activation. Moreover, the ability to work with unmodified receptors and G proteins (except for G_s) offers numerous advantages. First, it allows for the detection of endogenous GPCR signaling in either generic HEK293 cells (**Figure S8**) or more physiologically relevant cell lines such as induced pluripotent stem cell (iPSC)-derived cardiomyocytes (**Figure 7A**) and promyelocytic HL-60 cells (**Figure 7B**). Further it allows, in cells expressing sufficient endogenous level of the G proteins of interest, to detect activation of both native receptor and G proteins with no need of overexpression (**Figure 7C-D**). This is illustrated by the ability to detect the recruitment of Rap1GAP upon activation of the endogenous $G_{i/o}$ family members by the formyl peptide receptor 2 (FPR2) in HL-60 cells (**Figure 7C**) or protease-activated receptor-2 (PAR2) in HEK293 cells (**Figure 7D**). The ability to detect the activation of endogenous G protein was also illustrated in **Figure S1I**, where the responses elicited by agonist stimulation were lost in cells genetically deleted of the G protein engaged by the studied receptor (i.e.: $G_{q/11}$ or $G_{i/o}$ families). Recently, another BRET-based approach (Maziarz et al., 2020), taking advantage of a synthetic peptide recognizing the GTP-bound form of Gα subunits, also allows the

detection of native G protein activation offering alternative means to probe coupling selectivity profiles for both endogenously and heterologously expressed GPCRs.

Finally, similarly to BERKY, the EMTA assay platform detects the active form of the Gα subunits rather than the surrogate measurement of Gαβγ dissociation (Gales et al., 2005; Masuho et al., 2015; Maziarz et al., 2020; Mende et al., 2018), which can also detect non-productive binding as recently described for the V_2 engagement of G_{12} (Okashah et al., 2020).

A potential caveat of EMTA is the use of common downstream effectors for all members of a given G protein family. Indeed, one cannot exclude that distinct members of a given family may display different relative affinities for their common effector. However, such differences are compensated by our data normalization that establishes the maximal response observed for a given subtype as the reference for this pathway (**Figure 3A**), as long as the number of the diversity of receptors including in the analysis is sufficient.

A second potential caveat of EMTA is that, when using heterologously expressed GPCRs and G proteins, some of the responses could result from favorable stoichiometries that may not exist under physiological conditions. It follows that such profiling represents the coupling possibilities of a given GPCR and not necessarily the coupling that will be observed in all cell types. Any couplings observed in such high-throughput studies requires further validation to conclude on their physiological relevance in cells or tissues

of interest, and to form hypothesis for futures studies. Because we elected to use unmodified receptors (*i.e.*: not bearing any tags), the expression level of receptors could not be directly monitored. However, the double normalization method developed (see Methods) allows quantitative comparison of coupling preferences across different receptors curtailing the influence of the assay response windows as well as receptor expression levels. Indeed, the double normalization allows ranking the coupling propensity of the receptors first as a function of the receptor which shows the strongest coupling to a specific G protein subtype, and then establishing the maximal response observed for a given G protein subtype as the reference for all G protein activated by a given receptor. In addition, as illustrated using the ET_A receptor as example, titrating receptor levels did not influence the pEC_{50} for the activation of the different G protein coupled to this receptor (**Figure S3B** and **Supplementary Table 1C**). Similarly, the pEC_{50} was not affected when titrating the amount of G protein subtype expressed (**Figure S3A** and **Supplementary Table 1B**). As expected, only the amplitude of the response was affected.

It could be argued that overexpressing the G protein effectors (i.e.: p63-RhoGEF, Rap1GAP or PDZ-RhoGEF) used as sensors could influence the couplings observed. This potential caveat is mitigated by the fact that we used truncated part and/or modified versions of these effectors that limit the possibilities of interference with other components of the signaling machinery, and served essentially as a binding detector of the active forms of the G proteins (see Material and Methods). Supporting this notion,

titrating the amount of the biosensor effector component did not affect the pEC_{50} of G protein activation (**Figure S3C and Supplementary Table 1D**).

Another limitation of the EMTA platform is the lack of a soluble effector protein selective for activated $G\alpha_s$ thus requiring tagging of the $G\alpha_s$ subunit (**Figure 1B**, bottom) and monitoring its dissociation from the plasma membrane. Yet, our data show that this translocation reflects G_s activation state, justifying its use in a G protein activation detection platform.

Finally, because EMTA is able to detect constitutive activity, high receptor expression levels may lead to an elevated basal signal level that may obscure an agonist-promoted response. Such an example can be appreciated for the A_1 receptor for which the agonist-promoted $G\alpha_{i2}$ response did not reach the activation threshold criteria because of a very high constitutive activity level (**Figure 5A**). The impact of receptor expression on the constitutive activity and the narrowing on the agonist-promoted response is illustrated for $G\alpha_q$ activation by the $5\text{-}HT_{2C}$ (**Figure S11B**).

A limitation of any large-scale signaling study and drug discovery program is that ligands may elicit responses downstream of receptors other than the one under study. The development of a G_z/G_{15} quasi-universal biosensor enables efficient screening and detection of such polypharmacology and cross-talk. Using a combination of EMTA and appropriate pharmacological tools, we also proposed a systematic approach to

distinguish off-target action of ligands from cross-talk. Interestingly, the cross-talk between the M_3 and CB receptors detected (**Figure 6**) may have physiological relevance since activation of muscarinic acetylcholine receptors has been shown to enhance the release of endocannabinoids in the hippocampus (Kim, Isokawa, Ledent, & Alger, 2002). The combined G_z/G_{15} biosensor should be particularly useful for early profiling of compound activity on safety panels and for the design of drugs displaying polypharmacology, an approach that is increasingly considered for the development neuropsychiatric drugs (Roth et al., 2004).

The EMTA platform undoubtedly represents a novel tool-set that could be amenable for high throughput screening of small molecules and biologics across an array of signaling pathways, allowing for the discovery of functionally selective molecules or for GPCR deorphanization campaigns. The ability of the EMTA platform to quantitatively assess -G protein coupling selectivity firmly expands the concept of functional selectivity and potential ligand bias beyond the dichotomic G protein *vs.* βarrestin view and provides plausible functional selectivity profiles that could be tested for their biological and pharmacological outcomes.

Materials and Methods

Cells

HEK293 clonal cell line (HEK293SL cells), hereafter referred as HEK293 cells, were a gift from S. Laporte (McGill University, Montreal, Quebec, Canada) and previously described (Namkung et al., 2016). HEK293 cells devoid of functional $G\alpha_s$ (ΔG_s), $G\alpha_{12}$ and $G\alpha_{13}$ ($\Delta G_{12/13}$), $G\alpha_q$, $G\alpha_{11}$, $G\alpha_{14}$ and $G\alpha_{15}$ ($\Delta G_{q/11}$) and, $G\alpha_{i,}$ and $G\alpha_o$ ($\Delta G_{i/o}$) proteins were a gift from Dr. A. Inoue (Tohoku University, Sendai, Miyagi, Japan) and previously described (Devost et al., 2017; Namkung et al., 2018; Schrage et al., 2015; Stallaert et al., 2017). Cells were maintained in Dulbecco's Modified Eagle Medium (DMEM, Wisent, Saint-Jean-Baptiste, QC, Canada) supplemented with 10% fetal bovine serum (FBS, Wisent) and 1% antibiotics (100 U/mL penicillin and 100 µg/mL streptomycin (PS); Wisent). HL-60 cells were obtained from ATCC and maintained in RPMI 1640 medium containing L-Glutamine and 25 mM HEPES (Gibco) supplemented with 20% FBS (Wisent) and 1/100 volume PS (Wisent). Differentiation of HL-60 cells into neutrophil-like cells was induced by maintaining the cells in growth medium containing 1.3 % DMSO (Bioshop) during 5 days. Cardiomyocytes derived from induced pluripotent stem cells (iPSCs; iCell Cardiomyocytes) were obtained from FUJIFILM Cellular Dynamics (Madison, WI, USA) and maintained in maintenance medium provided with the cells (special formulation by FujiFilm). Cells were grown at 37°C in 5% CO_2 and 90% humidity and checked for mycoplasma contamination.

Plasmids and ebBRET biosensor constructs

555 Only human GPCRs and human Gα subunits were used in this study. An open reading
556 frame of each full-length GPCR was cloned into pcDNA3.1(+) expression plasmid. Except
557 when otherwise specified, GPCRs sequences were devoid of epitope tags.
558 $G\alpha_s$-67-RlucII (Carr et al., 2014), $G\alpha_{i1}$-loop-RlucII and GFP10-$G\gamma_1$ (Armando et al., 2014),
559 $G\alpha_{i2}$-loop-RlucII and βarrestin2-RlucII (Quoyer et al., 2013), $G\alpha_{oB}$-99-RlucII (Mende et al.,
560 2018), $G\alpha_q$-118-RlucII (Breton et al., 2010), $G\alpha_{12}$-136-RlucII and PKN-RBD-RlucII (Namkung
561 et al., 2018), $G\alpha_{13}$-130-RlucII (Avet et al., 2020), GFP10-$G\gamma_2$ (Gales et al., 2006), βarrestin1-
562 RlucII (Zimmerman et al., 2012), rGFP-CAAX (Namkung et al., 2016), EPAC (Leduc et al.,
563 2009), MyrPB-Ezrin-RlucII (Leguay et al., 2021), HA-β_2AR (Lavoie et al., 2002), signal
564 peptide-Flag-AT_1 (Goupil et al., 2015) and EAAC-1 (Brabet et al., 1998) were previously
565 described. Full-length, untagged Gα subunits, $G\beta_1$ and $G\gamma_9$ were purchased from cDNA
566 Resource Center. GRK2 was generously provided by Dr. Antonio De Blasi (Istituto
567 Neurologico Mediterraneo Neuromed, Pozzilli, Italy).
568
569 To selectively detect $G_{i/o}$ activation, a construct coding for aa 1-442 of Rap1 GTPase-
570 activating protein (comprising a $G_{i/o}$ binding domain) fused to Rluc8, was sequence-
571 optimized, synthetized and subcloned at TopGenetech (St-Laurent, QC, Canada). From
572 this construct, a RlucII tagged version of Rap1GAP (1-442) with a linker sequence
573 (GSAGTGGRAIDIKLPAT) between Rap1GAP and RlucII was created by Gibson assembly in
574 pCDNA3.1_Hygro (+) GFP10-RlucII, replacing GFP10. Three substitutions (i.e.,
575 S437A/S439A/S441A) were introduced into the Rap1GAP sequence by PCR-mediated
576 mutagenesis. These putative (S437 and S439) and documented (S441) (McAvoy, Zhou,

577 Greengard, & Nairn, 2009) protein kinase A phosphorylation sites were removed in order
578 to eliminate any G_s-mediated Rap1GAP recruitment to the plasma-membrane.
579 To selectively detect $G_{q/11}$ activation, a construct encoding the G_q binding domain of the
580 human p63 Rho guanine nucleotide exchange factor (p63RhoGEF; residues: 295-502)
581 tagged with RlucII was done from IMAGE clones (OpenBiosystems; Burlington, ON,
582 Canada) and subcloned by Gibson assembly in pCDNA3.1_Hygro (+) GFP10-RlucII,
583 replacing GFP10. The G_q binding domain of p63RhoGEF and RlucII were separated by the
584 peptidic linker ASGSAGTGGRAIDIKLPAT. N-term part containing palmitoylation sites
585 maintaining p63 to plasma membrane and part of its DH domain involved in RhoA
586 binding/activation (Aittaleb et al., 2010; Aittaleb, Nishimura, Linder, & Tesmer, 2011) are
587 absent of the sensor.
588 To selectively detect $G_{12/13}$ activation, a construct encoding the $G_{12/13}$ binding domain of
589 the human PDZ-RhoGEF (residues: 281-483) tagged with RlucII was done by PCR
590 amplification from IMAGE clones (OpenBiosystems) and subcloned by Gibson assembly
591 in pCDNA3.1_Hygro (+) GFP10-RlucII, replacing GFP10. The peptidic linker GIRLREALKLPAT
592 is present between RlucII and the $G_{12/13}$ binding domain of PDZ-RhoGEF. The sensor is
593 lacking the PDZ domain of PDZ-RhoGEF involved in protein-protein interaction, as well as
594 actin-binding domain and DH/PH domains involved in GEF activity and RhoA activation
595 (Aittaleb et al., 2010).
596
597 **Transfection**

For BRET experiments, HEK293 cells (1.2 mL at 3.5 × 10^5 cells per mL) were transfected with a fixed final amount of pre-mixed biosensor-encoding DNA (0.57 µg, adjusted with salmon sperm DNA; Invitrogen) and human receptor DNA. Transfections were performed using a polyethylenimine solution (PEI, 1 mg/mL; Polysciences, Warrington, PA, USA) diluted in NaCl (150 mM, pH 7.0; 3:1 PEI/DNA ratio). Gelatin solution (1%; Sigma-Aldrich, Saint-Louis, Missouri) was used to stabilize DNA/PEI transfection mixes. Following addition of cells to the stabilized DNA/PEI transfection mix, cells were immediately seeded (3.5 × 10^4 cells/well) into 96-well white microplates (Greiner Bio-one; Monroe, NC, USA) and maintained in culture for the next 48 h in DMEM containing 2% FBS and 1% PS. DMEM medium without L-glutamine (Wisent) was used for transfection of cells with mGluR to avoid receptor activation and desensitization. For Neutrophil-like differentiated HL-60 cells, cells were resuspended in electroporation medium (growth medium containing an extra 15 mM of HEPES pH 7.0) at 25 x 10^6 cells/mL. Electroporation reactions were prepared by adding 50 µL of DNA mastermix (20 µg total of DNA adjusted with salmon sperm DNA, supplemented with 210 mM NaCl) to 200 µL of cell suspension and transferring into 0.4 cm gap electroporation cuvettes (Bio-Rad). The cells were electroporated at 350 µF/400 V using a Bio-Rad Gene Pulser II electroporation system, washed in electroporation medium, and seeded in 96-well plates at 0.8 x 10^6 cells/well in 200 µL of growth medium. BRET assays were performed 6 hours post-electroporation. For iPSC Cardiomyocytes, cells were seeded in 96-well plates pretreated with fibronectin (10µg/ml 60 min; Sigma-Aldrich) at 3.5 × 10^4 cells /well. After 48 h, attached iPSCs cells were transfected with the indicated biosensor components, using TransIT-LT1 reagent

(Mirus; Madison, WI, USA), according to manufacturer recommendation. BRET assays were performed 48 hours after transfection.

For Ca^{2+} experiments, cells (3.5 x 10^4 cells/well) were co-transfected with the indicated receptor, with or without $G\alpha_{15}$ protein, using PEI and seeded in poly-ornithine coated 96-well clear-bottomed black microplates (Greiner Bio-one) and maintained in culture for the next 48 h.

For BRET-based imagery, cells (4 x 10^5 cells/dish) were seeded into 35-mm poly-d-lysine-coated glass-bottom culture dishes (Mattek Corporation; Ashland, MA, USA) in 2 ml of fresh medium and incubated at 37°C in 5% CO_2, 3 day before imaging experiments. Twenty-four hours later, cells were transfected with EMTA ebBRET biosensors and the indicated receptor (i.e., p63-RhoGEF-RlucII/rGFP-CAAX + $G\alpha_q$ and GnRHR, Rap1GAP-RlucII/rGFP-CAAX + $G\alpha_{i2}$ and D_2 or PDZ-RhoGEF-RlucII/rGFP-CAAX + $G\alpha_{13}$ and TPαR) using X-tremeGENE 9 DNA transfection reagent (3:1 reagent/DNA ratio; Roche) diluted in OptiMEM (Gibco) and maintained in culture for the next 48 h in DMEM containing 10% FBS and 1% PS.

Bioluminescence Resonance Energy Transfer Measurement

Enhanced bystander BRET (ebBRET) was used to monitor the activation of each Gα protein, as well as βarrestin 1 and 2 recruitment to the plasma membrane. $G\alpha_s$ protein activation was measured between the plasma membrane marker rGFP-CAAX and human $G\alpha_s$-RlucII in presence of human $G\beta_1$, $G\gamma_9$ and the tested receptor. $G\alpha_s$ downstream cAMP production was determined using the EPAC biosensor and GPBA receptor. $G\alpha_{i/o}$ protein

family activation was followed using the selective-$G_{i/o}$ effector Rap1GAP-RlucII and rGFP-CAAX along with the human $G\alpha_{i1}$, $G\alpha_{i2}$, $G\alpha_{oA}$, $G\alpha_{oB}$ or $G\alpha_{z}$ subunits and the tested receptor. $G\alpha_{q/11}$ protein family activation was determined using the selective-$G_{q/11}$ effector p63-RhoGEF-RlucII and rGFP-CAAX along with the human $G\alpha_{q}$, $G\alpha_{11}$, $G\alpha_{14}$ or $G\alpha_{15/16}$ subunits and the tested receptor. $G\alpha_{12/13}$ protein family activation was monitored using the selective-$G_{12/13}$ effector PDZ-RhoGEF-RlucII and rGFP-CAAX in presence of either $G\alpha_{12}$ or $G\alpha_{13}$ and the tested receptor. The expression level of the Gα subunits was monitored by Western blot in HEK293 cells that endogenously expressed $G\alpha_{i1}$, $G\alpha_{i2}$, $G\alpha_{12}$, $G\alpha_{13}$, $G\alpha_{q}$, $G\alpha_{11}$, $G\alpha_{14}$ and Gαs but not $G\alpha_{oA}$, $G\alpha_{oB}$, $G\alpha_{z}$ and $G\alpha_{15}$ (**Figure S6**). $G\alpha_{12/13}$-downstream activation of the Rho pathway was measured using PKN-RBD-RlucII and rGFP-CAAX with the indicated receptor. βarrestin recruitment to the plasma membrane was determined using DNA mix containing rGFP-CAAX and βarrestin1-RlucII with GRK2 or βarrestin2-RlucII alone or with GRK2 and the tested receptor. Glutamate transporters EAAC-1 and EAAT-1 were systematically co-transfected with the mGluR to prevent receptor activation and desensitization by glutamate secreted in the medium by the cells (Brabet et al., 1998). All ligands were also tested for potential activation of endogenous receptors by transfecting the biosensors without receptor DNA. The G_z/G_{15} biosensor consists of a combination of the following plasmids: rGFP-CAAX, Rap1GAP-RlucII, $G\alpha_{z}$, p63-RhoGEF-RlucII and $G\alpha_{15}$. For G protein activation detection using the BRET-based Gαβγ dissociation sensors, cells were co-transfected with untagged $G\beta_1$ and $G\alpha_{q}$-118-RlucII, $G\alpha_{12}$-136-RlucII or $G\alpha_{13}$-130-RlucII with GFP10-$G\gamma_1$, or $G\alpha_{i1}$-loop-RlucII, $G\alpha_{i2}$-loop-RlucII or $G\alpha_{oB}$-99-RlucII with GFP10-$G\gamma_2$, along with the indicated receptor.

The day of the BRET experiment, cells were incubated in HBSS for 1 h at room temperature (RT). Cells were then co-treated with increasing concentrations of ligand (see **Supplementary Table 2** for details) and the luciferase substrate coelenterazine prolume purple (1 µM, NanoLight Technologies; Pinetop, AZ, USA) for 10 min at RT. Plates were read on a Synergy Neo microplate reader (BioTek Instruments, Inc.; Winooski, VT, USA) equipped with 410 ± 80 nm donor and 515 ± 30 nm acceptor filters or with a Spark microplate reader (Tecan; Männedorf, Switzerland) using the $BRET^2$ manufacturer settings. The BRET signal ($BRET^2$) was determined by calculating the ratio of the light intensity emitted by the acceptor over the light intensity emitted by the donor. To validate the specificity of the biosensor responses, cells were pretreated in the absence or presence of either the $G\alpha_q$ inhibitor UBO-QIC (100 nM, 30 min; Institute for Pharmaceutical Biology of the University of Bonn, Germany), the $G\alpha_{i/o}$ inhibitor PTX (100 ng/mL, 18 h; List Biological Laboratories, Campbell, California, USA) or the $G\alpha_s$ activator CTX (0 to 200 ng/mL, 4h; Sigma-Aldrich) before stimulation with agonist. For Inverse agonist activity detection of A_1 or CB_1 receptors, cells were stimulated during 10 min with increasing concentrations of DPCPX or rimonabant, respectively. For ligand-cross receptor activation experiments, cells were pretreated for 10 min with increasing concentrations of antagonists or inverse agonist (eticlopride for D_2, WB4101 for $\alpha_{2A}AR$, atropine for muscarinic receptors and AM-630 for CB_1) before a 10 min stimulation with an EC_{80} concentration of the indicated agonist. BRET was measured as described above. For the safety target panel ligand screen using the combined G_z/G_{15} sensor, basal ebBRET level

686 was first measured 10 min following addition of coelenterazine prolume purple (1 µM)
687 and ebBRET level was measured again following a 10 min stimulation with a single dose
688 of the indicated ligand (1 µM for endothelin-1 and 10 µM for all other ligands). Technical
689 replicates for each receptor were included on the same 96-well plate. For kinetics
690 experiment of ET_A activation, basal BRET was measured during 150 sec before cells
691 stimulation with either vehicle (DMSO) or 1 µM of endothelin-1 (at time 0 sec) and BRET
692 signal was recorded each 30 sec during 3570 sec. For the validation of $G_{12/13}$-mediated
693 signal by new identified $G_{12/13}$-coupled receptor using PKN- or Ezrin-based BRET
694 biosensors, cells were pretreated or not with the $G\alpha_q$ inhibitor YM-254890 (1 µM, 30 min;
695 Wako Pure Chemical Industries; Wako Pure Chemical Industries (Fujifilm), Osaka, Japan)
696 before agonist stimulation for 10 min. For G protein activation detection using the BRET-
697 based Gαβγ dissociation sensors, and for titration experiments of either Gα proteins
698 subunit with GEMTA sensors, GPCRs with GEMTA sensors or Effector-RlucII (p63-RhoGEF-
699 RlucII for $G\alpha_{q/11}$, Rap1GAP-RlucII for $G\alpha_{i/o}$ or PDZ-RhoGEF-RlucII for $G\alpha_{12/13}$) from GEMTA
700 sensors, cells were stimulated with increasing concentrations of the indicated agonist in
701 presence of prolume purple for 10 min before BRET measurement. For BRET in iPSC
702 Cardiomyocytes and HL-60 cells, cells were incubated in Tyrode Hepes buffer (137 mM
703 NaCl, 0.9 mM KCl, 1 mM $MgCl_2$, 11.9 mM $NaHCO_3$, 3.6 mM NaH_2PO_4, 25 mM HEPES, 5.5
704 mM D-Glucose and 1 mM $CaCl_2$, pH 7.4) 30 min at RT before to be treated with increasing
705 concentration of agonist for 15 min, using prolume purple (2 µM) as luciferase substrate,
706 and BRET measured.
707

BRET Data analyses and coupling efficiency evaluation

All BRET ratios were standardized using the equation below and represented as universal BRET (*u*BRET) values: *u*BRET = ((BRET ratio – A)/(B-A)) * 10 000. Constants A and B correspond to the following values:

A = pre-established BRET ratio obtained from transfection of negative control (vector coding for RlucII alone);

B = pre-established BRET ratio obtained from transfection of positive control (vector coding for a GFP10-RlucII fusion protein).

For a given signaling pathway, *u*BRET values at each agonist concentration were normalized as the % of the response obtained in the absence of agonist (vehicle) and concentration-response curves were fitted in GraphPad Prism 8 software using a four-parameter logistic nonlinear regression model. Results are expressed as mean ± SEM of at least three independent experiments.

A ligand-promoted response was considered real when the E_{max} value was ≥ to the mean + 2*SD of the response obtained in vehicle condition and that a pEC_{50} value could be determined in the agonist concentration range used to stimulate the receptor. Consequently, a score of 0 or 1 was assigned to each signaling pathway depending on an agonist's ability to activate the tested pathway (0= no activation; 1= activation). In the case were responses associated to endogenous receptor were detectable, we considered as "distorted" and exclude all the responses observed in the presence of transfected

receptor for which E_{max} was ≤ to 2*mean of the E_{max} value obtained with endogenous receptors or pEC_{50} was ≥ to 2*mean of the pEC_{50} value obtained with endogenous receptors. Consequently, a score of 0 was assigned for these distorted responses in radial graph representation (**Figure S7**) and dose-response curves were placed on a gray background in signaling signature profile panels (**Supplementary File 1**). Whenever transfected receptors produced an increase in E_{max} or a left-shift in pEC_{50} values compared to endogenous receptors, responses were considered 'true' and were assigned with a score of 1 for radial graph representation (**Figure S7**) and dose-response curves were placed on a yellow background in signaling signature profile panels to indicate a partial contribution of endogenous receptors (**Supplementary File 1**).

We used a double normalization of E_{max} and pEC_{50} values to compare the signaling efficiency obtained for the 100 GPCRs across all receptors and pathways. E_{max} and pEC_{50} values deduced from concentration-response curves were first normalized between 0 and 1 across receptors by ranking the receptors as a function of the receptor that most efficiently activate a given pathway and then using the activation value for the pathway (including G protein and βarrestin subtypes) that a given receptor most efficiently activate as a reference for the other pathways that can be activated by this receptor. This double normalization can be translated in the following formalized equation:

- STEP1: For each receptor and for each pathway:

$$\left[\frac{E_{max}\ GPCR_x}{E_{max}\ GPCR_{Ref}}\right]_{Pathway\ A} = Pathway\ specific\ normalized\ score\ for\ GPCR_x\ on\ pathway\ A\ ([PSNS\ GPCR_x]_{Pathway\ A})$$

Where: $GPCR_x$ is receptor being analyzed, $GPCR_{Ref}$ is the receptor giving greatest E_{max} on pathway A of all receptors studied (i.e., reference receptor for pathway A). A PSNS was determined for every receptor and every pathway coupled to that receptor.

- STEP2: For any given receptor:

$$\frac{[PSNS\ GPCR_x]_{\ Pathway\ A}}{[PSNS\ GPCR_x]_{\ Ref\ pathway}} = \textit{Normalized pathway A coupling score for } GPCR_x$$

Where: $[PSNS\ GPCR_x]_{\ Pathway\ A}$ is the pathway specific normalized score for $GPCR_x$ on pathway A, and $[PSNS\ GPCR_x]_{\ Ref\ pathway}$ is the pathway specific normalized score for the pathway giving the highest PSNS for $GPCR_x$ (i.e., reference pathway for $GPCR_x$).

For the safety target panel ligand screen using the combined G_z/G_{15} sensor, the fold ligand-induced stimulation was calculated for each receptor by dividing the BRET ratio after ligand addition (measured at 10 minutes post stimulation) by the basal BRET ratio prior to receptor stimulation. Activation thresholds were defined as the mean + 2*SD of the ligand-stimulated response obtained with receptor-null cells expressing only the combined G_z/G_{15} sensor.

Ca^{2+} mobilization assay

The day of experiment, cells were incubated with 100 µL of a Ca^{2+}-sensitive dye-loading buffer (FLIPR calcium 5 assay kit, Molecular Devices; Sunnyvale, CA, USA) containing 2.5 mM probenecid (Sigma-Aldrich) for 1 h at 37°C in a 5% CO_2 incubator. During a data run,

cells in individual wells were exposed to an EC_{80} concentration of agonist, and fluorescent signals were recorded every 1.5 s for 3 min using the FlexStation II microplate reader (Molecular Devices). For receptors that also activate other $G_{q/11}$ family members, cells were pretreated with the $G_{q/11}$ inhibitor YM-254890 (1 µM, 30 min) before agonist stimulation. $G\alpha_{15}$ is resistant to inhibition by YM-254890, thus allowing to measure Ca^{2+} responses generated specifically by $G\alpha_{15}$.

BRET-based imaging

BRET images were obtained as previously described (Kobayashi, Picard, Schonegge, & Bouvier, 2019). Briefly, the day of imaging experiment, cells were carefully rinsed with HBSS, and images were acquired before and after agonists addition (100 nM for GnRH and U46619, and 1 µM for dopamine) diluted in HBSS in presence of the luciferase substrate coelenterazine prolume purple (20 µM).

Images were recorded using an inverted microscope (Nikon Eclipse Ti-U) equipped with x60 objective lens (Nikon CFI Apochromat TIRF) and EM-CCD camera (Nuvu HNu 512). Measurements were carried out in photon counting mode with EM gain 3,000. Exposure time of each photon counting was 100 ms. Successive 100 frames were acquired alternatively with 480 nm longpass filter (acceptor frames) or without filter (total luminescence frames), and integrated. Image integrations were repeated 5 times and 500 frames of acceptor and total luminescence were used to generate each image.

BRET values were obtained by dividing acceptor counts by total luminescence counts pixelwise. BRET values from 0.0 to 0.5 were allocated to 'jet' heatmap array using MATLAB

2019b. Brightness of each pixel was mapped from the signal level of total luminescence image. 0% and 99.9% signal strength were allocated to the lowest and highest brightness to exclude the influence of defective pixels with gamma correction factor of 2.0.

The movies were generated using ImageJ 1.52a. Frame rate is 3 frames/sec, and frame interval is 100 sec. The field of view of the movie is 137 um x 137 um.

Western blot analysis

Cells were transfected or not with the indicated biosensors mix as previously described and whole-cell extracts were prepared 48 h later. Briefly, cells were washed with ice-cold PBS and lysed in a buffer containing 10 mM Tris buffer (pH 7.4), 100 mM NaCl, 1 mM EDTA, 1 mM EGTA, 0.1% SDS, 1% Triton X-100, 10% Glycerol supplemented with protease inhibitors cocktails (Thermo Fisher Scientific). Cell lysates were centrifuged at 13,000 × g for 30 min at 4°C. Equal amounts of proteins were separated by SDS-PAGE and transferred onto polyvinylidene fluoride membrane. The membranes were blocked in (incubation 1 hr at room temperature in PBS 0.1% Tween-20, 5% BSA) and successively probed with primary antibody and appropriate goat secondary antibodies coupled to horseradish peroxidase (described in table below). Western blots were visualized using enhanced chemiluminescence and detection was performed using a ChemiDoc MP Imaging System (BioRad). Relative densitometry analysis on protein bands was performed using MultiGauge software (Fujifilm). Results were normalized against control bands.

Target	Dilution	Species	Class	Reference	Manufacturer
Gαi1 (I-20)	1:500	Rabbit	polyclonal	#sc-391	Santa Cruz

Gαi2 (T-19)	1:500	Rabbit	polyclonal	#sc-7276	Santa Cruz
Gαo (K-20)	1:500	Rabbit	polyclonal	#sc-387	Santa Cruz
Gαz	1:1,000	Rabbit	monoclonal	# ab154846	Abcam
Gαs (K-20)	1:500	Rabbit	polyclonal	#sc-823	Santa Cruz
Gα12 (S-20)	1:500	Rabbit	polyclonal	#sc-409	Santa Cruz
Gα13 (A-20)	1:500	Rabbit	polyclonal	#sc-410	Santa Cruz
Gαq (E-17)	1:500	Rabbit	polyclonal	#sc-393	Santa Cruz
Gα11 (C-terminal)	1:500	Rabbit	Polyclonal	#SAB2109181	Sigma-Aldrich
Gα14	1:500	Rabbit	Polyclonal	#SAB4300771	Sigma-Aldrich
Gα15	1:5,000	Rabbit	Polyclonal	#PA1-29022	ThermoFisher scientific (Pierce)
βactin	1:5,000	Mouse	Monoclonal	#A5441	Sigma-Aldrich
Anti-rabbit HRP-coupled	1:5,000	Donkey	Polyclonal	#NA934	GE Healthcare
Anti-mouse HRP-coupled	1:10,000	Sheep	Polyclonal	#NA931	GE Healthcare

816

817 **Statistical Analyses**

818 Curve fitting and statistical analyses were performed using GraphPad Prism 9.3 software
819 and methods are described in the legends of the figures. Significance was determined as
820 $p < 0.05$.

References

Aittaleb, M., Boguth, C. A., & Tesmer, J. J. (2010). Structure and function of heterotrimeric G protein-regulated Rho guanine nucleotide exchange factors. *Mol Pharmacol, 77*(2), 111-125. doi:10.1124/mol.109.061234

Aittaleb, M., Nishimura, A., Linder, M. E., & Tesmer, J. J. (2011). Plasma membrane association of p63 Rho guanine nucleotide exchange factor (p63RhoGEF) is mediated by palmitoylation and is required for basal activity in cells. *J Biol Chem, 286*(39), 34448-34456. doi:10.1074/jbc.M111.273342

Armando, S., Quoyer, J., Lukashova, V., Maiga, A., Percherancier, Y., Heveker, N., . . . Bouvier, M. (2014). The chemokine CXC4 and CC2 receptors form homo- and heterooligomers that can engage their signaling G-protein effectors and betaarrestin. *FASEB J, 28*(10), 4509-4523. doi:10.1096/fj.13-242446

Atwood, B. K., Lopez, J., Wager-Miller, J., Mackie, K., & Straiker, A. (2011). Expression of G protein-coupled receptors and related proteins in HEK293, AtT20, BV2, and N18 cell lines as revealed by microarray analysis. *BMC Genomics, 12*, 14. doi:10.1186/1471-2164-12-14

Avet, C., Sturino, C., Grastilleur, S., Gouill, C. L., Semache, M., Gross, F., . . . Bouvier, M. (2020). The PAR2 inhibitor I-287 selectively targets Galphaq and Galpha12/13 signaling and has anti-inflammatory effects. *Commun Biol, 3*(1), 719. doi:10.1038/s42003-020-01453-8

Azzi, M., Charest, P. G., Angers, S., Rousseau, G., Kohout, T., Bouvier, M., & Pineyro, G. (2003). Beta-arrestin-mediated activation of MAPK by inverse agonists reveals distinct active conformations for G protein-coupled receptors. *Proc Natl Acad Sci U S A, 100*(20), 11406-11411. doi:10.1073/pnas.1936664100

Bowes, J., Brown, A. J., Hamon, J., Jarolimek, W., Sridhar, A., Waldron, G., & Whitebread, S. (2012). Reducing safety-related drug attrition: the use of in vitro pharmacological profiling. *Nat Rev Drug Discov, 11*(12), 909-922. doi:10.1038/nrd3845

Brabet, I., Parmentier, M. L., De Colle, C., Bockaert, J., Acher, F., & Pin, J. P. (1998). Comparative effect of L-CCG-I, DCG-IV and gamma-carboxy-L-glutamate on all cloned metabotropic glutamate receptor subtypes. *Neuropharmacology, 37*(8), 1043-1051. doi:10.1016/s0028-3908(98)00091-4

Breton, B., Sauvageau, E., Zhou, J., Bonin, H., Le Gouill, C., & Bouvier, M. (2010). Multiplexing of multicolor bioluminescence resonance energy transfer. *Biophys J, 99*(12), 4037-4046. doi:10.1016/j.bpj.2010.10.025

Bunemann, M., Frank, M., & Lohse, M. J. (2003). Gi protein activation in intact cells involves subunit rearrangement rather than dissociation. *Proc Natl Acad Sci U S A, 100*(26), 16077-16082. doi:10.1073/pnas.2536719100

Carr, R., 3rd, Du, Y., Quoyer, J., Panettieri, R. A., Jr., Janz, J. M., Bouvier, M., . . . Benovic, J. L. (2014). Development and characterization of pepducins as Gs-biased allosteric agonists. *J Biol Chem, 289*(52), 35668-35684. doi:10.1074/jbc.M114.618819

Casey, P. J., Fong, H. K., Simon, M. I., & Gilman, A. G. (1990). Gz, a guanine nucleotide-binding protein with unique biochemical properties. *J Biol Chem, 265*(4), 2383-2390. Retrieved from https://www.ncbi.nlm.nih.gov/pubmed/2105321

Chandan N.R., A. S., SenGupta S., Parent C.A., Smrcka A.V. (2021). Identification of G Protein αi Signaling Partners by Proximity Labeling Reveals a Network of Interactions that Includes PDZ-RhoGEF. *bioRxiv preprint*. doi:https://doi.org/10.1101/2021.07.15.452545

De Haan, L., & Hirst, T. R. (2004). Cholera toxin: a paradigm for multi-functional engagement of cellular mechanisms (Review). *Mol Membr Biol, 21*(2), 77-92. doi:10.1080/09687680410001663267

Devost, D., Sleno, R., Petrin, D., Zhang, A., Shinjo, Y., Okde, R., . . . Hebert, T. E. (2017). Conformational Profiling of the AT1 Angiotensin II Receptor Reflects Biased Agonism, G Protein Coupling, and Cellular Context. *J Biol Chem, 292*(13), 5443-5456. doi:10.1074/jbc.M116.763854

875 Fukuhara, S., Chikumi, H., & Gutkind, J. S. (2001). RGS-containing RhoGEFs: the missing
876 link between transforming G proteins and Rho? *Oncogene, 20*(13), 1661-1668.
877 doi:10.1038/sj.onc.1204182
878 Galandrin, S., Oligny-Longpre, G., & Bouvier, M. (2007). The evasive nature of drug
879 efficacy: implications for drug discovery. *Trends Pharmacol Sci, 28*(8), 423-430.
880 doi:10.1016/j.tips.2007.06.005
881 Gales, C., Rebois, R. V., Hogue, M., Trieu, P., Breit, A., Hebert, T. E., & Bouvier, M. (2005).
882 Real-time monitoring of receptor and G-protein interactions in living cells. *Nat*
883 *Methods, 2*(3), 177-184. doi:10.1038/nmeth743
884 Gales, C., Van Durm, J. J., Schaak, S., Pontier, S., Percherancier, Y., Audet, M., . . . Bouvier,
885 M. (2006). Probing the activation-promoted structural rearrangements in
886 preassembled receptor-G protein complexes. *Nat Struct Mol Biol, 13*(9), 778-786.
887 doi:10.1038/nsmb1134
888 Goupil, E., Fillion, D., Clement, S., Luo, X., Devost, D., Sleno, R., . . . Hebert, T. E. (2015).
889 Angiotensin II type I and prostaglandin F2alpha receptors cooperatively modulate
890 signaling in vascular smooth muscle cells. *J Biol Chem, 290*(5), 3137-3148.
891 doi:10.1074/jbc.M114.631119
892 Hauser, A. S., Attwood, M. M., Rask-Andersen, M., Schioth, H. B., & Gloriam, D. E. (2017).
893 Trends in GPCR drug discovery: new agents, targets and indications. *Nat Rev Drug*
894 *Discov, 16*(12), 829-842. doi:10.1038/nrd.2017.178
895 Hauser, A. S., Avet, C., Normand, C., Mancini, A., Inoue, A., Bouvier, M., & Gloriam, D. E.
896 (2021). GPCR-G protein selectivity - a unified meta-analysis *bioRxiv*.
897 doi:https://doi.org/10.1101/2021.09.07.459250
898 Hoffmann, C., Gaietta, G., Bunemann, M., Adams, S. R., Oberdorff-Maass, S., Behr, B., . . .
899 Lohse, M. J. (2005). A FlAsH-based FRET approach to determine G protein-coupled
900 receptor activation in living cells. *Nat Methods, 2*(3), 171-176. doi:10.1038/nmeth742
901 Inoue, A., Raimondi, F., Kadji, F. M. N., Singh, G., Kishi, T., Uwamizu, A., . . . Russell, R. B.
902 (2019). Illuminating G-Protein-Coupling Selectivity of GPCRs. *Cell, 177*(7), 1933-1947
903 e1925. doi:10.1016/j.cell.2019.04.044

904 Jordan, J. D., Carey, K. D., Stork, P. J., & Iyengar, R. (1999). Modulation of rap activity by
905 direct interaction of Galpha(o) with Rap1 GTPase-activating protein. *J Biol Chem, 274*(31), 21507-21510. doi:10.1074/jbc.274.31.21507
906
907 Kawamata, Y., Fujii, R., Hosoya, M., Harada, M., Yoshida, H., Miwa, M., . . . Fujino, M.
908 (2003). A G protein-coupled receptor responsive to bile acids. *J Biol Chem, 278*(11),
909 9435-9440. doi:10.1074/jbc.M209706200
910 Kenakin, T. (2019). Biased Receptor Signaling in Drug Discovery. *Pharmacol Rev, 71*(2),
911 267-315. doi:10.1124/pr.118.016790
912 Kim, J., Isokawa, M., Ledent, C., & Alger, B. E. (2002). Activation of muscarinic
913 acetylcholine receptors enhances the release of endogenous cannabinoids in the
914 hippocampus. *J Neurosci, 22*(23), 10182-10191. Retrieved from
915 https://www.ncbi.nlm.nih.gov/pubmed/12451119
916 Kobayashi, H., Picard, L. P., Schonegge, A. M., & Bouvier, M. (2019). Bioluminescence
917 resonance energy transfer-based imaging of protein-protein interactions in living cells.
918 *Nat Protoc, 14*(4), 1084-1107. doi:10.1038/s41596-019-0129-7
919 Laschet, C., Dupuis, N., & Hanson, J. (2019). A dynamic and screening-compatible
920 nanoluciferase-based complementation assay enables profiling of individual GPCR-G
921 protein interactions. *J Biol Chem, 294*(11), 4079-4090. doi:10.1074/jbc.RA118.006231
922 Lavoie, C., Mercier, J. F., Salahpour, A., Umapathy, D., Breit, A., Villeneuve, L. R., . . .
923 Hebert, T. E. (2002). Beta 1/beta 2-adrenergic receptor heterodimerization regulates
924 beta 2-adrenergic receptor internalization and ERK signaling efficacy. *J Biol Chem, 277*(38), 35402-35410. doi:10.1074/jbc.M204163200
925
926 Leduc, M., Breton, B., Gales, C., Le Gouill, C., Bouvier, M., Chemtob, S., & Heveker, N.
927 (2009). Functional selectivity of natural and synthetic prostaglandin EP4 receptor
928 ligands. *J Pharmacol Exp Ther, 331*(1), 297-307. doi:10.1124/jpet.109.156398
929 Leguay, K., Decelle, B., He, Y. Y., Pagniez, A., Hogue, M., Kobayashi, H., . . . Carreno, S.
930 (2021). Development of conformational BRET biosensors that monitor ezrin, radixin
931 and moesin activation in real time. *J Cell Sci, 134*(7). doi:10.1242/jcs.255307

Lu, M., Wang, B., Zhang, C., Zhuang, X., Yuan, M., Wang, H., . . . Li, J. (2014). PQ-69, a novel and selective adenosine A1 receptor antagonist with inverse agonist activity. *Purinergic Signal, 10*(4), 619-629. doi:10.1007/s11302-014-9424-5

Lutz, S., Shankaranarayanan, A., Coco, C., Ridilla, M., Nance, M. R., Vettel, C., . . . Tesmer, J. J. (2007). Structure of Galphaq-p63RhoGEF-RhoA complex reveals a pathway for the activation of RhoA by GPCRs. *Science, 318*(5858), 1923-1927. doi:10.1126/science.1147554

Mancini, A., Frauli, M., & Breton, B. (2015). Exploring the Technology Landscape of 7TMR Drug Signaling Profiling. *Curr Top Med Chem, 15*(24), 2528-2542. doi:10.2174/1568026615666150701113344

Martin, B. R., & Lambert, N. A. (2016). Activated G Protein Galphas Samples Multiple Endomembrane Compartments. *J Biol Chem, 291*(39), 20295-20302. doi:10.1074/jbc.M116.729731

Masuho, I., Ostrovskaya, O., Kramer, G. M., Jones, C. D., Xie, K., & Martemyanov, K. A. (2015). Distinct profiles of functional discrimination among G proteins determine the actions of G protein-coupled receptors. *Sci Signal, 8*(405), ra123. doi:10.1126/scisignal.aab4068

Maziarz, M., Park, J. C., Leyme, A., Marivin, A., Garcia-Lopez, A., Patel, P. P., & Garcia-Marcos, M. (2020). Revealing the Activity of Trimeric G-proteins in Live Cells with a Versatile Biosensor Design. *Cell, 182*(3), 770-785 e716. doi:10.1016/j.cell.2020.06.020

McAvoy, T., Zhou, M. M., Greengard, P., & Nairn, A. C. (2009). Phosphorylation of Rap1GAP, a striatally enriched protein, by protein kinase A controls Rap1 activity and dendritic spine morphology. *Proc Natl Acad Sci U S A, 106*(9), 3531-3536. doi:10.1073/pnas.0813263106

Mende, F., Hundahl, C., Plouffe, B., Skov, L. J., Sivertsen, B., Madsen, A. N., . . . Holst, B. (2018). Translating biased signaling in the ghrelin receptor system into differential in vivo functions. *Proc Natl Acad Sci U S A, 115*(43), E10255-E10264. doi:10.1073/pnas.1804003115

960 Meng, J., Glick, J. L., Polakis, P., & Casey, P. J. (1999). Functional interaction between
961 Galpha(z) and Rap1GAP suggests a novel form of cellular cross-talk. *J Biol Chem, 274*(51), 36663-36669. doi:10.1074/jbc.274.51.36663
962
963 Namkung, Y., Le Gouill, C., Lukashova, V., Kobayashi, H., Hogue, M., Khoury, E., . . .
964 Laporte, S. A. (2016). Monitoring G protein-coupled receptor and beta-arrestin
965 trafficking in live cells using enhanced bystander BRET. *Nat Commun, 7*, 12178.
966 doi:10.1038/ncomms12178
967 Namkung, Y., LeGouill, C., Kumar, S., Cao, Y., Teixeira, L. B., Lukasheva, V., . . . Laporte, S.
968 A. (2018). Functional selectivity profiling of the angiotensin II type 1 receptor using
969 pathway-wide BRET signaling sensors. *Sci Signal, 11*(559).
970 doi:10.1126/scisignal.aat1631
971 Okashah, N., Wright, S. C., Kawakami, K., Mathiasen, S., Zhou, J., Lu, S., . . . Lambert, N. A.
972 (2020). Agonist-induced formation of unproductive receptor-G12 complexes. *Proc Natl*
973 *Acad Sci U S A, 117*(35), 21723-21730. doi:10.1073/pnas.2003787117
974 Oldham, W. M., & Hamm, H. E. (2008). Heterotrimeric G protein activation by G-protein-
975 coupled receptors. *Nat Rev Mol Cell Biol, 9*(1), 60-71. doi:10.1038/nrm2299
976 Olsen, R. H. J., DiBerto, J. F., English, J. G., Glaudin, A. M., Krumm, B. E., Slocum, S. T., . . .
977 Strachan, R. T. (2020). TRUPATH, an open-source biosensor platform for interrogating
978 the GPCR transducerome. *Nat Chem Biol, 16*(8), 841-849. doi:10.1038/s41589-020-
979 0535-8
980 Quoyer, J., Janz, J. M., Luo, J., Ren, Y., Armando, S., Lukashova, V., . . . Bouvier, M. (2013).
981 Pepducin targeting the C-X-C chemokine receptor type 4 acts as a biased agonist
982 favoring activation of the inhibitory G protein. *Proc Natl Acad Sci U S A, 110*(52), E5088-
983 5097. doi:10.1073/pnas.1312515110
984 Rojas, R. J., Yohe, M. E., Gershburg, S., Kawano, T., Kozasa, T., & Sondek, J. (2007). Galphaq
985 directly activates p63RhoGEF and Trio via a conserved extension of the Dbl homology-
986 associated pleckstrin homology domain. *J Biol Chem, 282*(40), 29201-29210.
987 doi:10.1074/jbc.M703458200

988 Roth, B. L., Sheffler, D. J., & Kroeze, W. K. (2004). Magic shotguns versus magic bullets:
989 selectively non-selective drugs for mood disorders and schizophrenia. *Nat Rev Drug*
990 *Discov, 3*(4), 353-359. doi:10.1038/nrd1346
991 Sanchez-Soto, M., Bonifazi, A., Cai, N. S., Ellenberger, M. P., Newman, A. H., Ferre, S., &
992 Yano, H. (2016). Evidence for Noncanonical Neurotransmitter Activation:
993 Norepinephrine as a Dopamine D2-Like Receptor Agonist. *Mol Pharmacol, 89*(4), 457-
994 466. doi:10.1124/mol.115.101808
995 Schrage, R., Schmitz, A. L., Gaffal, E., Annala, S., Kehraus, S., Wenzel, D., . . . Kostenis, E.
996 (2015). The experimental power of FR900359 to study Gq-regulated biological
997 processes. *Nat Commun, 6*, 10156. doi:10.1038/ncomms10156
998 Stallaert, W., van der Westhuizen, E. T., Schonegge, A. M., Plouffe, B., Hogue, M.,
999 Lukashova, V., . . . Bouvier, M. (2017). Purinergic Receptor Transactivation by the
1000 beta2-Adrenergic Receptor Increases Intracellular Ca(2+) in Nonexcitable Cells. *Mol*
1001 *Pharmacol, 91*(5), 533-544. doi:10.1124/mol.116.106419
1002 Sunahara, R. K., Guan, H. C., O'Dowd, B. F., Seeman, P., Laurier, L. G., Ng, G., . . . Niznik, H.
1003 B. (1991). Cloning of the gene for a human dopamine D5 receptor with higher affinity
1004 for dopamine than D1. *Nature, 350*(6319), 614-619. doi:10.1038/350614a0
1005 Takasaki, J., Saito, T., Taniguchi, M., Kawasaki, T., Moritani, Y., Hayashi, K., & Kobori, M.
1006 (2004). A novel Galphaq/11-selective inhibitor. *J Biol Chem, 279*(46), 47438-47445.
1007 doi:10.1074/jbc.M408846200
1008 Wedegaertner, P. B., Bourne, H. R., & von Zastrow, M. (1996). Activation-induced
1009 subcellular redistribution of Gs alpha. *Mol Biol Cell, 7*(8), 1225-1233.
1010 doi:10.1091/mbc.7.8.1225
1011 Wei, H., Ahn, S., Shenoy, S. K., Karnik, S. S., Hunyady, L., Luttrell, L. M., & Lefkowitz, R. J.
1012 (2003). Independent beta-arrestin 2 and G protein-mediated pathways for angiotensin
1013 II activation of extracellular signal-regulated kinases 1 and 2. *Proc Natl Acad Sci U S A,*
1014 *100*(19), 10782-10787. doi:10.1073/pnas.1834556100
1015 Zimmerman, B., Beautrait, A., Aguila, B., Charles, R., Escher, E., Claing, A., . . . Laporte, S.
1016 A. (2012). Differential beta-arrestin-dependent conformational signaling and cellular

responses revealed by angiotensin analogs. *Sci Signal, 5*(221), ra33. doi:10.1126/scisignal.2002522

Acknowledgments

We thank Shane C. Wright for scientific discussion and Monique Lagacé for critical reading of the manuscript. The authors are grateful to the funding from Bristol-Myers Squibb that supported the detection of Gα proteins by endogenous receptors in iPSC cardiomyocytes and promyelocytic HL-60 cells.

Funding

Canada Research Chair in Signal Transduction and Molecular Pharmacology (MB)

Canadian Institutes of Health Research grant FDN-148431 (MB)

Lundbeck Foundation grants R218-2016-1266 and R313-2019-526 (DEG)

Novo Nordisk Foundation grant NNF18OC0031226 (DEG)

Author contributions

Conceptualization: CA, AM, BB, CLG, XL, MB

Methodology: CA, AM, BB, CLG, MB

Investigation: CA, AM, BB, CN, HK, FG, MH, VL, SS-O, MC, MH, SM

Formal Analysis: CA, AM, ASH, DEG, MB

Resources: AM, EF, J-PF, SS, XL, MB

Supervision: MH, XL, DEG, MB

Funding Acquisition: SS, DEG, MB

Writing: CA, AM, DEG, MB; All coauthors revised the manuscript

Competing interests

AM, BB, CN, FG and SM were employees of Domain Therapeutics North America during part or all of this research.

EF and J-FF are employees and shareholders of Pfizer.

SS and XL are employees and are part of the management of Domain Therapeutics.

MB is the president of Domain Therapeutics scientific advisory board.

BB, CLG, HK, MH, VL, MB have filed patent applications related to the biosensors used in this work and the technology has been licensed to Domain Therapeutics.

CA, ASH, SS-O, MC, MH and DEG have no competing interests to declare.

Data and materials availability

Further information and requests for resources and reagents should be directed to and will be fulfilled upon reasonable request by the Lead Contact, Michel Bouvier (michel.bouvier@umontreal.ca).

The ebBRET sensors used in the study are protected by patent applications and have been licensed to Domain Therapeutics. Inquiries for potential commercial use should be addressed to: xleroy@domaintherapeutics.com. For non-commercial academic use, the sensors can be obtained freely under material transfer agreement upon request to: michel.bouvier@umontreal.ca.

Heatmaps in **Figure 3** were generated using custom python scripts. Scripts are available from the co-corresponding author, David E. Gloriam (david.gloriam@sund.ku.dk) on request.

Figures

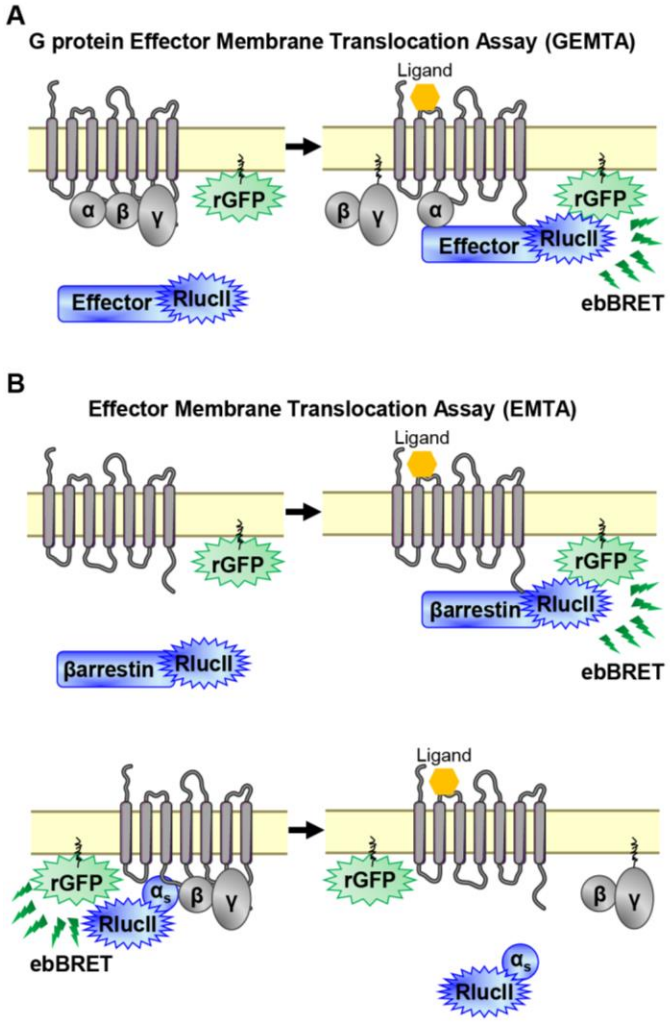

Figure 1. EMTA ebBRET platform to monitor G protein activation and βarrestin recruitment. (**A**) Schematic of the G protein Effector Membrane Translocation Assay (GEMTA) to monitor Gα protein activation. Upon receptor activation, RlucII-tagged effector proteins (Effector-RlucII) translocate towards and interact with active Gα subunits from each G protein family, leading to increased ebBRET. (**B**) Principle of the Effector Membrane Translocation Assay (EMTA) monitoring βarrestin recruitment to the plasma membrane (*top*) and $G\alpha_s$ activation (*bottom*). *Top*; upon receptor activation, RlucII-tagged βarrestins (βarrestin-RlucII) translocate to the plasma membrane, thus increasing ebBRET with rGFP-CAAX. *Bottom*; Internalization of activated RlucII-tagged $G\alpha_s$ ($G\alpha_s$-RlucII) following receptor stimulation decreases ebBRET with the membrane-anchored rGFP-CAAX.

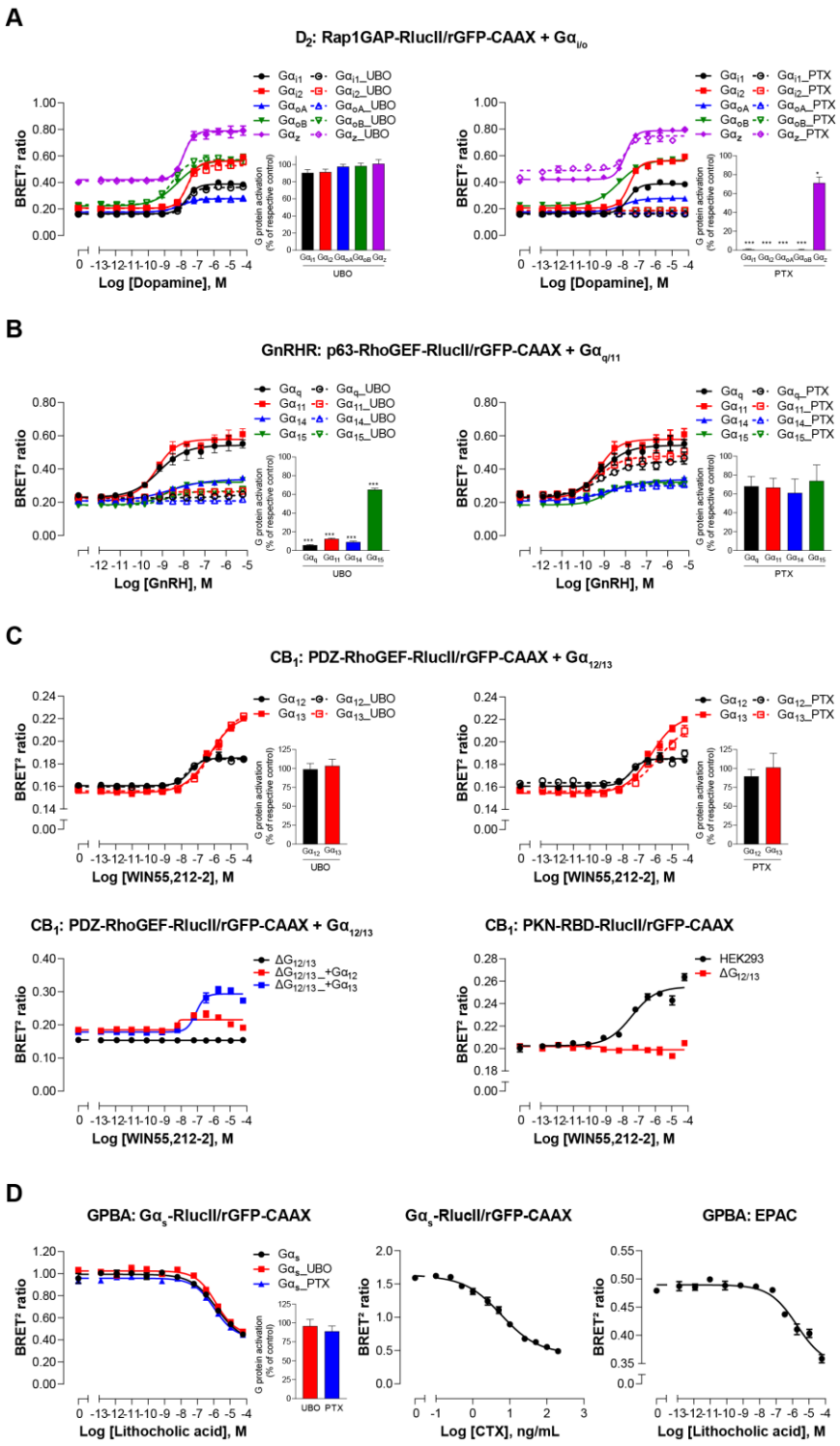

Figure 2. Validation of EMTA ebBRET-based platform to monitor Gα protein activation. (**A**) Pharmacological validation of the $G\alpha_{i/o}$ activation sensor. HEK293 cells were transfected with the D_2 receptor and the $G\alpha_{i/o}$ family-specific sensor, along with each $G\alpha_{i/o}$ subunit. Dose-response curve using the $G\alpha_{i/o}$ activation sensor, in the presence or absence of UBO-QIC (*left*) or PTX (*right*) inhibitors. *Insets*; E_{max} values determined from dose-response curves of inhibitor-pretreated cells. (**B**) Pharmacological validation of the $G\alpha_{q/11}$ activation sensor. HEK293 cells were transfected with the GnRH receptor and the $G\alpha_{q/11}$ family-

specific sensors, along with each $G\alpha_{q/11}$ subunit. Dose-response curve using $G\alpha_{q/11}$ activation sensor, in the presence or absence of UBO-QIC (*left*) or PTX (*right*) inhibitors. *Insets*; E_{max} values determined from dose-response curves of inhibitor-pretreated cells. (**C**) Validation of the $G\alpha_{12/13}$ activation sensor. Cells were transfected with the CB_1 receptor and one of the $G\alpha_{12/13}$ activation sensors, along with the $G\alpha_{12}$ or $G\alpha_{13}$ subunits. Dose-response curves of HEK293 cells (*top*) or the parental and devoid of $G_{12/13}$ ($\Delta G_{12/13}$) HEK293 cells (*bottom*) using the PDZ-RhoGEF-RlucII/rGFP-CAAX sensors (*top and bottom left*) or PKN-RBD-RlucII/rGFP-CAAX (*bottom right*), pretreated or not with UBO-QIC or PTX (*top*). (**D**) Pharmacological validation of the $G\alpha_s$ activation sensor. HEK293 cells were transfected with the GPBA receptor and the $G\alpha_s$ activation (*left and central*) or the EPAC (*right*) sensors. *Left:* Dose-response curves using the $G\alpha_s$ activation sensor in the presence or absence of UBO-QIC or PTX, inhibitors of $G\alpha_q$ or $G\alpha_{i/o}$, respectively. *Central*: Dose-response activation of the $G\alpha_s$ sensor using CTX, a $G\alpha_s$ activator. *Right*: Dose-response curve using the EPAC sensor. *Inset*; E_{max} values determined from dose-response curves of inhibitors-pretreated cells. Data are expressed as BRET ratio for the dose-response curves or expressed in % of respective control cells (E_{max} graphs) and are means ± SEM of 3 (**A**-**C**) or 4 (**D**) independent experiments performed in one replicate. Unpaired t-test (**A**-**D**): *$p < 0.05$ and ***$p < 0.001$ compared to control cells.

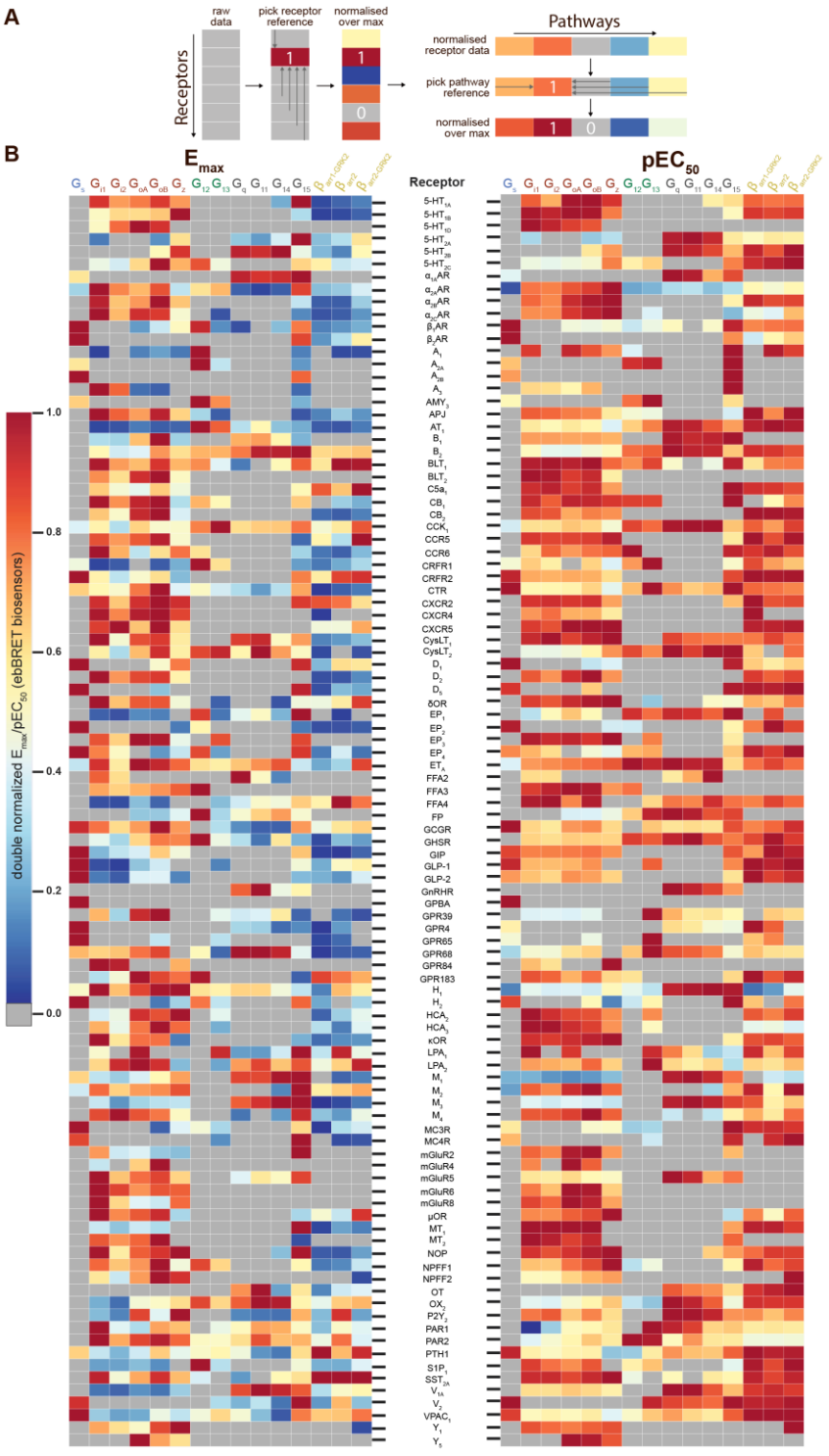

Figure 3. Heatmaps illustrating the diversity of receptor-specific signaling signatures detected with the EMTA ebBRET platform. (**A**) First, values within each pathway were normalized relative to the maximal response observed across all receptors (max = 1; *left*). These values were then normalized across pathways for the same receptor, with the highest-ranking pathway serving as the reference (max = 1; *right*). (**B**) Heatmap representation of double normalized E_{max} (*left*) and pEC_{50} (*right*) data. Empty cells (grey) indicate no detected coupling. IUPHAR receptor names are displayed.

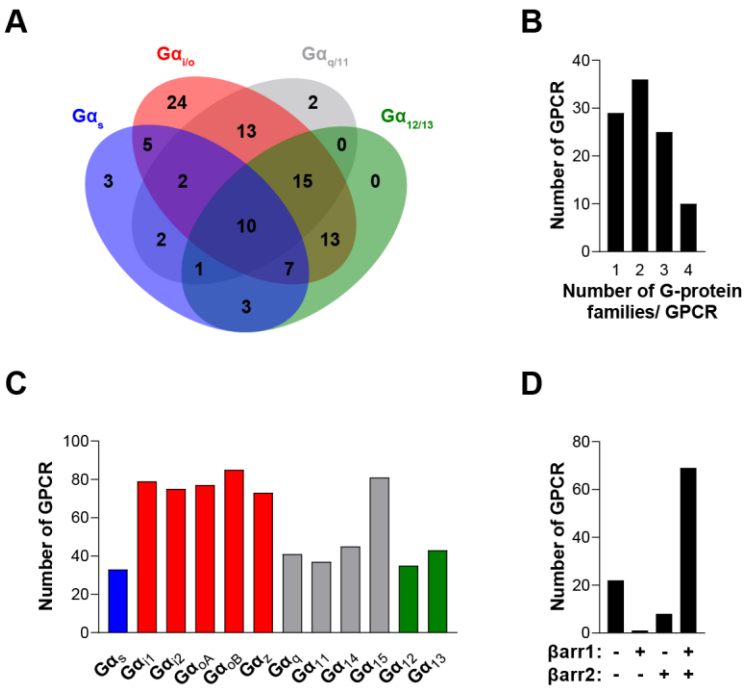

Figure 4. The EMTA ebBRET platform has a unique ability to uncover coupling selectivity between G protein families. (**A**) Venn diagram showing the numbers of receptors coupled to each G protein family in the EMTA ebBRET biosensor assay. (**B**) Evaluation of receptors coupling promiscuity: number of receptors that couple to members of 1, 2, 3 or 4 G protein families. (**C**) Determination of G protein subunit coupling frequency: number of receptors that activate each Gα subunit. (**D**) Proportion of receptors recruiting βarrestins: number of receptors that do not recruit (-/-) or that recruit either (+/- or -/+) or both (+/+) βarrestin isotypes. All data are based on double normalized E_{max} values from **Figure 3**.

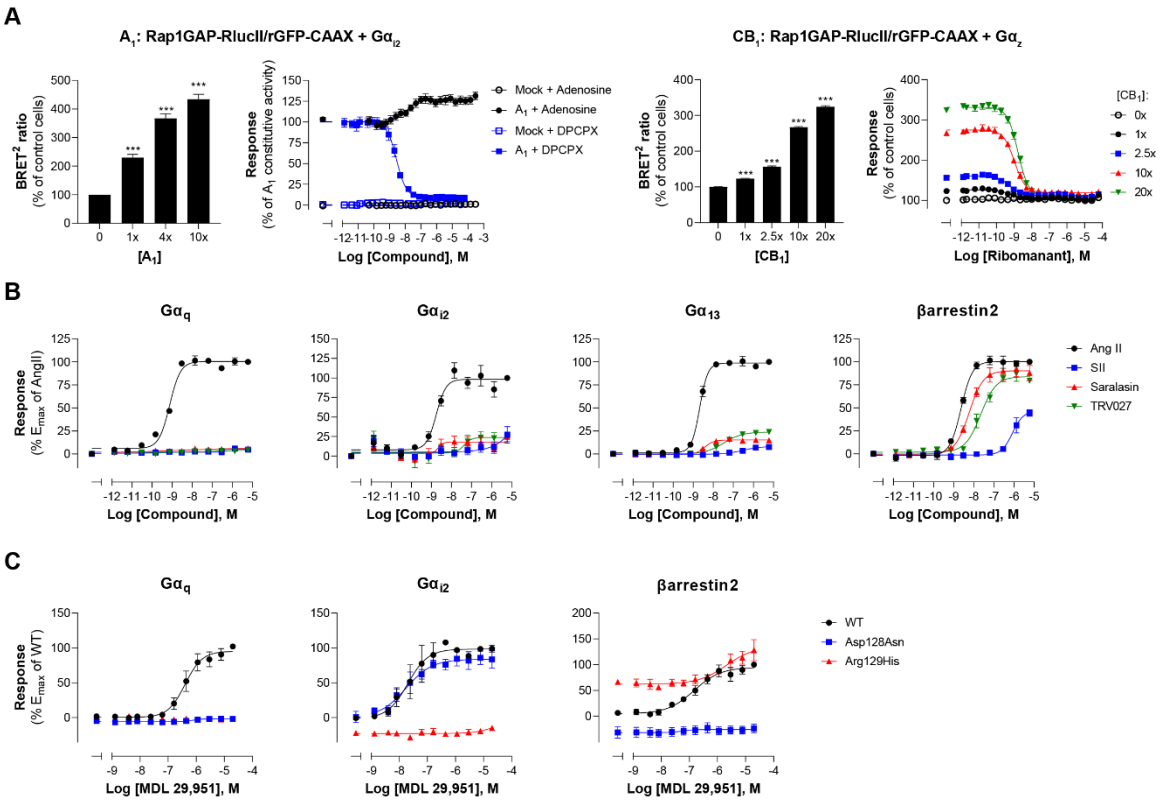

Figure 5. Multiple applications using the EMTA ebBRET platform. (**A**) Inverse agonist activity detection. *Left*: $G\alpha_{i2}$ activation in HEK293 cells transfected with the Rap1GAP-RlucII/rGFP-CAAX sensors with untagged $G\alpha_{i2}$ and increasing amount of A_1 receptor plasmid. Data are expressed in % of response obtained in control cells (0 ng of A_1) and are means ± SEM of 4-6 independent experiments performed in two replicates. One Way ANOVA test: ***$p < 0.001$ compared to control cells. HEK293 cells expressing the $G\alpha_{i2}$ activation sensor and control (Mock) or A_1 receptor plasmid were stimulated (10 min) with increasing concentrations of the indicated compound. Data are expressed in % of constitutive response obtained in vehicle-treated A_1 transfected cells and are means ± SEM of 4-6 independent experiments performed in one replicate. *Right:* $G\alpha_z$ activation in HEK293 cells transfected with the Rap1GAP-RlucII/rGFP-CAAX sensors with untagged $G\alpha_z$ and increasing amount of CB_1 receptor plasmid. Data are expressed in % of response obtained in control cells (0 ng of CB_1) and are means ± SEM of 4 independent experiments performed in one replicate. One Way ANOVA test: ***$p < 0.001$ compared to control cells. HEK293 cells expressing the $G\alpha_z$ activation sensor and increasing amount of CB_1 receptor plasmid were directly stimulated (10 min) with increasing concentrations of the CB_1 inverse agonist rimonabant. Data are expressed as % of the response obtained in control cells (0 ng of CB_1) treated with vehicle and are means ± SEM of 4 independent experiments performed in one replicate. (**B**) Ligand-biased detection. Concentration-response curves of AT_1 for the endogenous ligand (Angiotensin II, AngII) and biased agonists [Sar1-Ile4-Ile8] AngII (SII), saralasin or TRV027. G-protein and βarrestin2 signaling activity were assessed by EMTA platform. Data are expressed in % of maximal response elicited by AngII and are means ± SEM of 3-6 independent experiments performed in one replicate. (**C**) Functional selectivity of naturally occurring receptor variants. Concentration-response curves for WT or E/DRY motif Asp128Asn and Arg129His variants of GPR17 upon agonist stimulation in HEK293 cells co-expressing the indicated EMTA biosensor. Data are expressed in % of maximal response elicited by WT receptor and are means ± SEM of 3 independent experiments performed in one replicate.

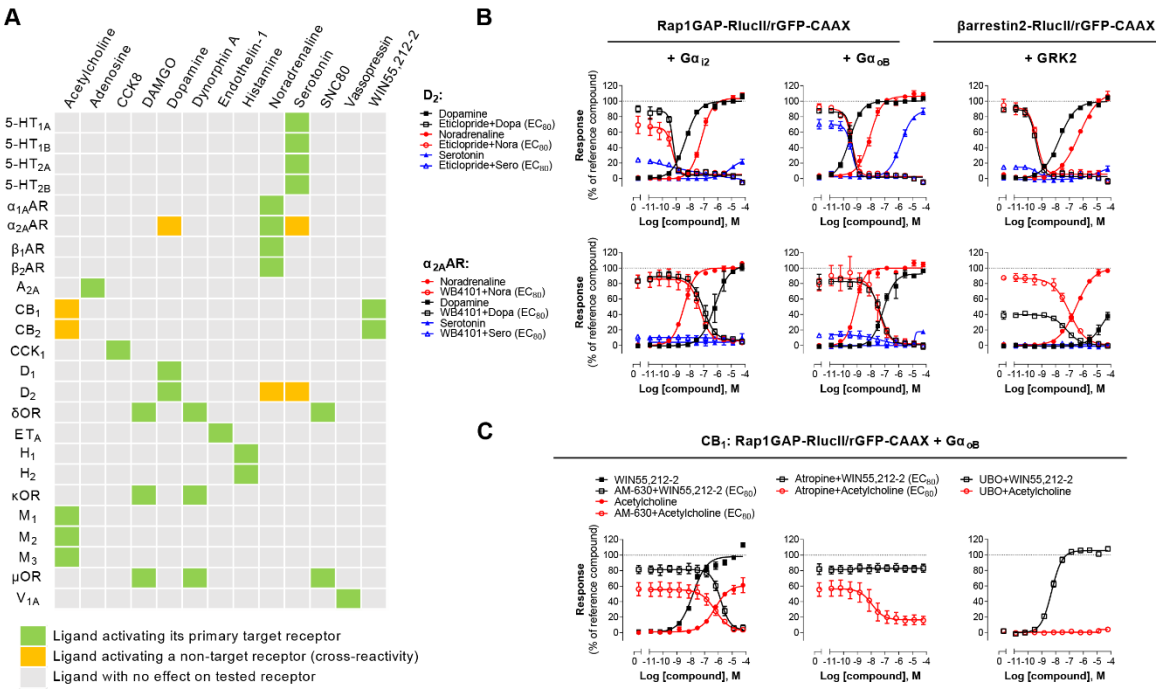

Figure 6. Detection of direct and indirect (*trans*) mechanisms of ligand polypharmacology using the G_z/G_{15} biosensor. (**A**) Test of the G_z/G_{15} biosensor on a safety target panel. ebBRET signal was measured before and after stimulation with the indicated ligand in HEK293 cells transfected with the combined G_z/G_{15} biosensor and one of the 24 receptors listed. (**B**) Cross-activation of D_2 and $\alpha_{2A}AR$ by others natural ligands. For the agonist mode read, HEK293 cells expressing D_2 or $\alpha_{2A}AR$ and either the $G\alpha_{i2}$, $G\alpha_{oB}$, or the βarrestin2+GRK2 sensors were stimulated with increasing concentrations of the indicated ligand. For the antagonist mode read, cells were pretreated with increasing concentrations of the selective D_2 antagonist eticlopride or the selective $\alpha_{2A}AR$ antagonist WB4101 before stimulation with an EC_{80} of the indicated ligand. Data are means ± SEM from 3-4 independent experiments performed in one replicate and expressed in % of the response elicited by dopamine or noradrenaline for D_2 and $\alpha_{2A}AR$ expressing cells, respectively. (**C**) Indirect (*trans*) activation of CB_1 by acetylcholine. For the agonist mode read, HEK293 cells expressing CB_1 and the Rap1GAP-RlucII/rGFP-CAAX sensors with untagged $G\alpha_{oB}$ were stimulated with increasing concentrations of the indicated ligand. For the antagonist mode read, same cells were pretreated or not with increasing concentrations of the CB inverse agonist AM-630 (*left*) or the cholinergic antagonist atropine (*central*) before stimulation with an EC_{80} of the indicated ligand. To evaluate the contribution of $G_{q/11}$-coupled receptor, cells were pretreated with the $G\alpha_q$ inhibitor UBO-QIC and then stimulated with increasing concentrations of the indicated ligand (*right*). Data are means ± SEM from 3-5 independent experiments performed in one replicate and expressed in % of the response elicited by WIN55,212-2.

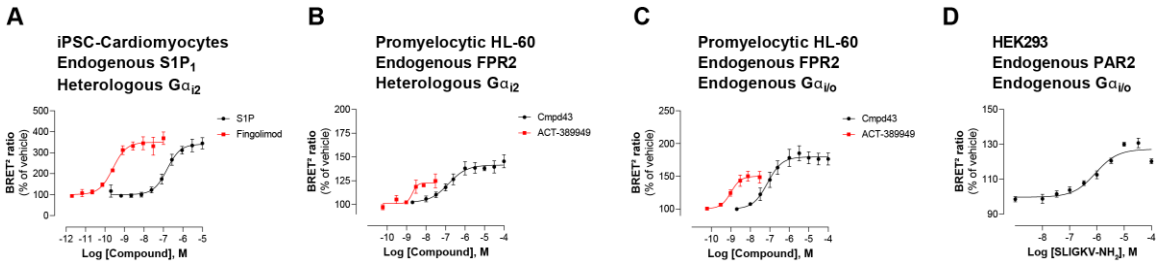

Figure 7. Detection of endogenous receptor- and/or G protein-mediated responses in cells with the EMTA ebBRET platform. Concentration-dependent activation of $G\alpha_{i2}$ protein by (**A**) endogenous $S1P_1$ receptor in iPSC-derived cardiomyocytes transfected with heterologous $G\alpha_{i2}$, (**B**) endogenous FPR2 in promyelocytic HL-60 cells transfected with heterologous $G\alpha_{i2}$, (**C**) endogenous FPR2 in promyelocytic HL-60 cells with endogenous $G_{i/o}$ proteins and (**D**) endogenous PAR2 receptor in HEK293 cells with endogenous $G_{i/o}$ proteins. In all cases, cells were co-transfected with the Rap1GAP-RlucII/rGFP-CAAX biosensor. Data are the mean ± SEM of 3-4 independent experiments performed in one replicate and are expressed as $BRET^2$ ratio in percentage of response induced by vehicle.

Supplementary Information for: Effector membrane translocation biosensors reveal G protein and βarrestin coupling profiles of 100 therapeutically relevant GPCRs

Charlotte Avet[1†], Arturo Mancini[2†], Billy Breton[2‡§], Christian Le Gouill[1‡], Alexander S. Hauser[3‡], Claire Normand[2], Hiroyuki Kobayashi[1], Florence Gross[2], Mireille Hogue[1], Viktoriya Lukasheva[1], Stéphane St-Onge[1], Marilyn Carrier[1], Madeleine Héroux[1], Sandra Morissette[2], Eric Fauman[4], Jean-Philippe Fortin[5], Stephan Schann[6], Xavier Leroy[6*], David E. Gloriam[3*], and Michel Bouvier[1*].

[1]*Institute for Research in Immunology and Cancer (IRIC), and Department of Biochemistry and Molecular Medicine, Université de Montréal; Montréal, Québec, H3T 1J4, Canada.*
[2]*Domain Therapeutics North America; Montréal, Québec, H4S 1Z9, Canada.*
[3]*Department of Drug Design and Pharmacology; University of Copenhagen; 2100 Copenhagen, Denmark.*
[4]*Internal Medicine Research Unit; Pfizer Worldwide Research, Development and Medical; Cambridge, MA 02139, USA.*
[5]*Pfizer Global R&D; Cambridge, MA 02139, USA.*
[6]*Domain Therapeutics; 67400 Illkirch-Strasbourg, France.*
[†]*These authors contributed equally.*
[‡]*These authors contributed equally.*
[§]*Current address: Institute for Research in Immunology and Cancer (IRIC), Université de Montréal; Montréal, Québec, H3T 1J4, Canada.*

*** Corresponding authors**:

Michel Bouvier ; IRIC, Université de Montréal : michel.bouvier@umontreal.ca,

David E. Gloriam; University of Copenhagen: david.gloriam@sund.ku.dk,

Xavier Leroy; Domain Therapeutics: xleroy@domaintherapeutics.com

Supplementary Figures

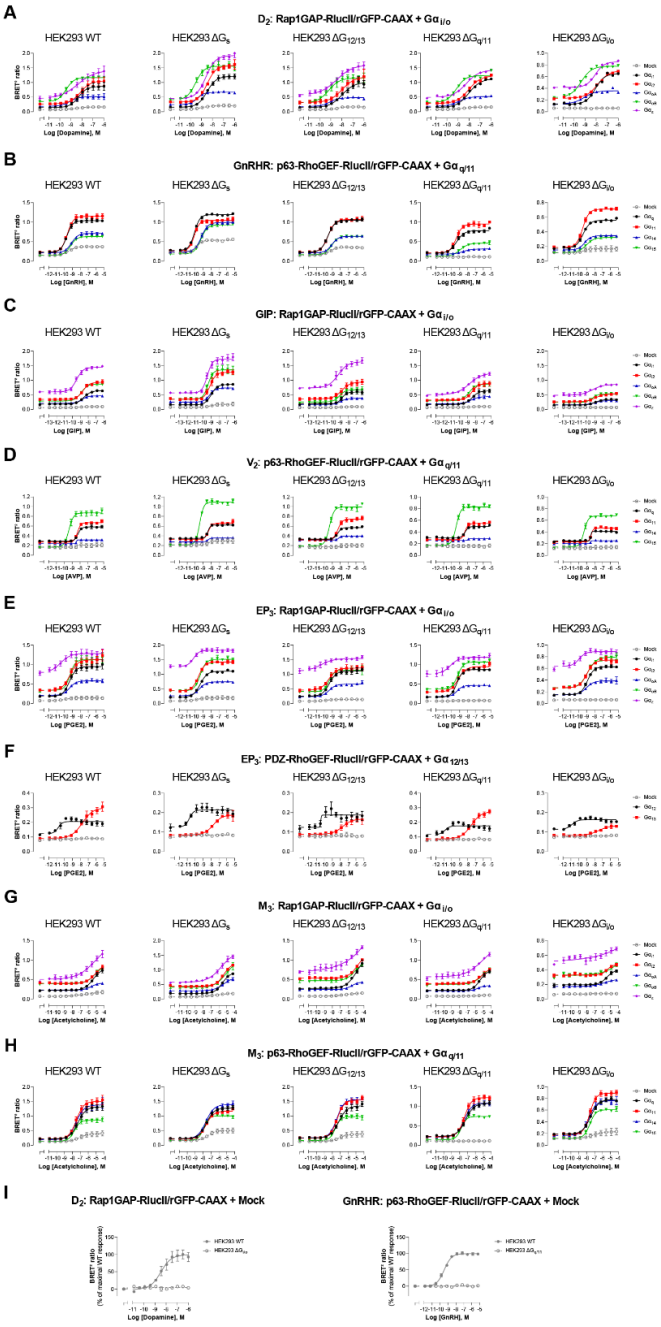

Figure S1. Influence of endogenous G proteins. Dose-response curves elicited in parental (WT) HEK293 cells or devoid of G_s (ΔG_s), $G_{12/13}$ ($\Delta G_{12/13}$), $G_{q/11}$ ($\Delta G_{q/11}$) or $G_{i/o}$ ($\Delta G_{i/o}$) proteins, transfected with the indicated receptor (D_2, GnRHR, GIP, V_2, EP_3 or M_3) and one of the $G\alpha_{i/o}$, $G\alpha_{q/11}$ or $G\alpha_{12/13}$ activation sensors, along with the indicated Gα subunits. Mock condition corresponded to the response elicited in absence of heterologously expressed Gα subunits (i.e., endogenous G proteins effect). Data are means ± SEM of 3-5 independent experiments performed in one replicate and are expressed as $BRET^2$ ratio. Data presented in **I** are the same as in **A**-**B**, but with results expressed as % of maximal response elicited by endogenous G proteins (mock) in WT cells.

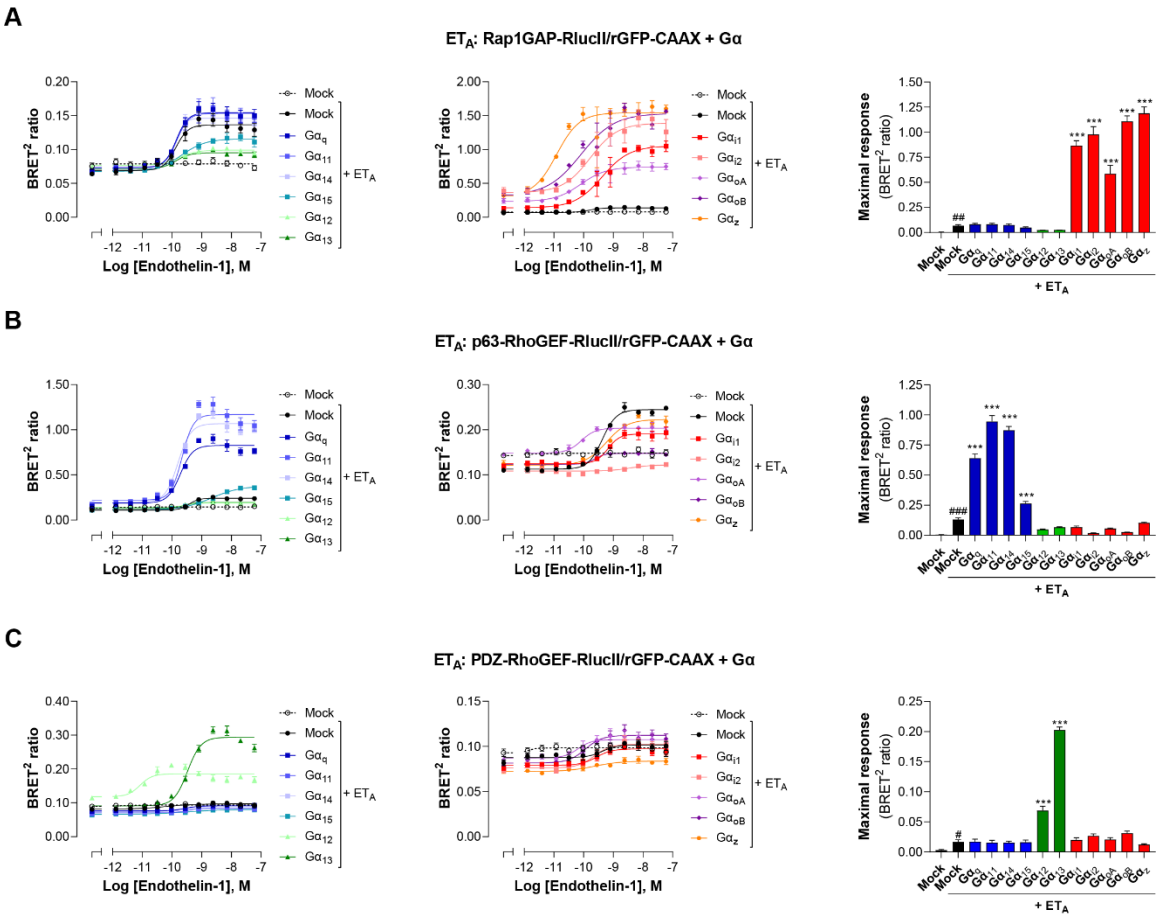

Figure S2. **Validation of EMTA ebBRET-based sensors selectivity for each Gα subunit families.** HEK293 cells were transfected with the ET_A receptor and $G\alpha_{i/o}$ (A), $G\alpha_{q/11}$ (B) or $G\alpha_{12/13}$ (C) activation sensors along with each Gα subunit or control DNA (Mock) as control for response obtained with endogenous Gα proteins. Dose-response curves in response to endothelin-1 are shown (*left and central*), as well as maximal responses obtained with each Gα subunit. Data are means ± SEM of 3 independent experiments performed in one replicate and are expressed as $BRET^2$ ratio. Unpaired t-test: $^{\#}p < 0.05$, $^{\#\#}p < 0.01$ and $^{\#\#\#}p < 0.001$ compared to Mock (without receptor) and One-Way ANOVA test: $*p < 0.05$, $**p < 0.01$ and $***p < 0.001$ compared to Mock + ET_A.

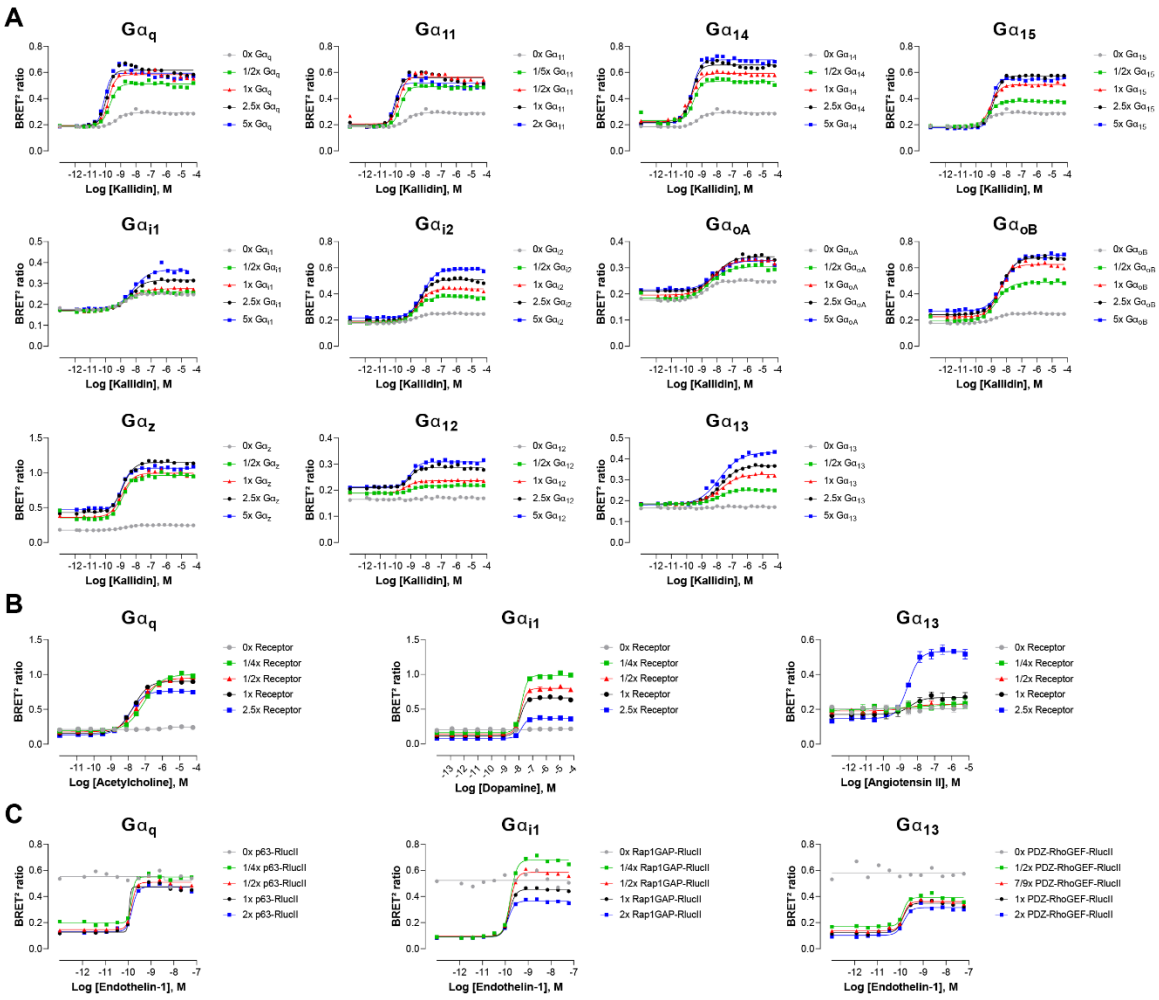

Figure S3. Influence of G protein, GPCR or effector-RlucII level expression. (**A**) Dose-response curves elicited in HEK293 cells transfected with the B_2 receptor and one of the $G\alpha_{q/11}$, $G\alpha_{i/o}$ or $G\alpha_{12/13}$ activation sensors, along with increasing quantity of the indicated Gα subunits. Data represent a representative experiment (**B**) Dose-response curves elicited in HEK293 cells transfected with increasing quantity of the M_3, D_2 or AT_1 receptors and the $G\alpha_{q/11}$, $G\alpha_{i/o}$ or $G\alpha_{12/13}$ activation sensors, along with the indicated Gα subunits. (**C**) Dose-response curves elicited in HEK293 cells transfected with the ET_A receptor and increasing quantity of effector-RlucII (p63-RhoGEF for $G\alpha_{q/11}$, Rap1GAP for $G\alpha_{i/o}$ or PDZ-RhoGEF for $G\alpha_{12/13}$), along with rGFP-CAAX and the indicated Gα subunits. Data are means ± SEM of 3 independent experiments performed in one replicate and are expressed in $BRET^2$ ratio.

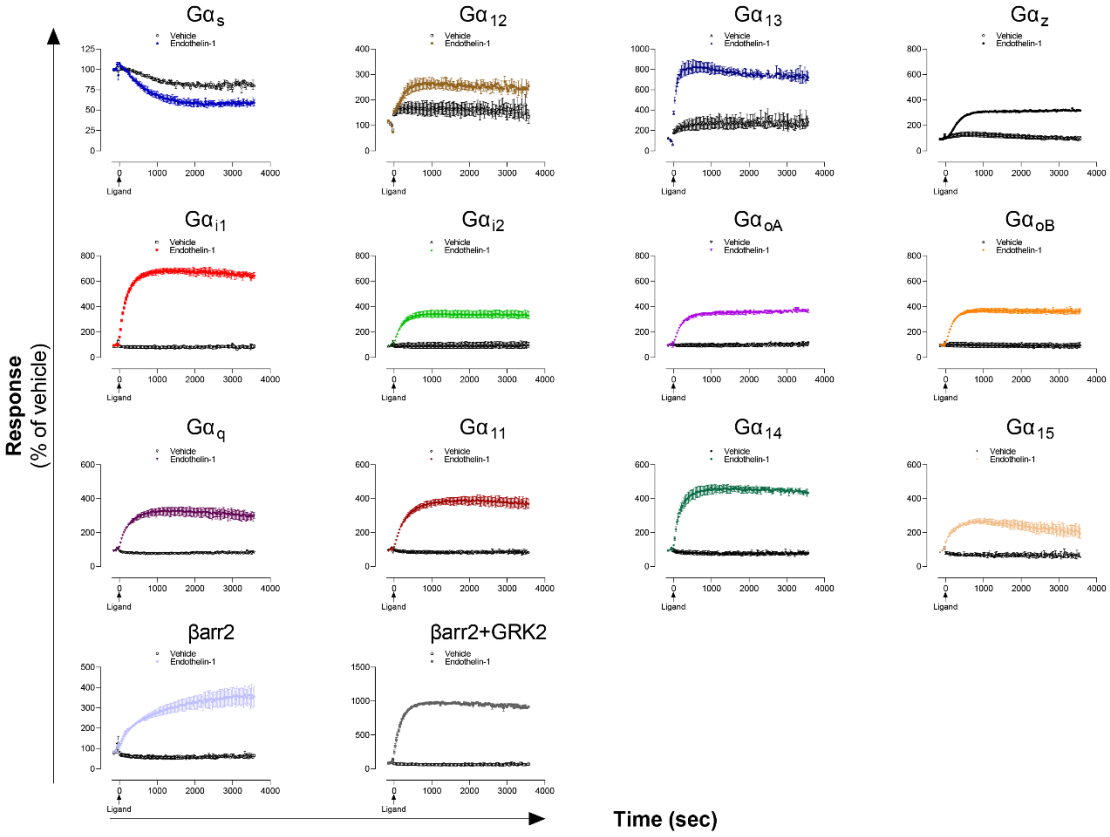

Figure S4. Kinetics of Gα proteins and βarrestins recruitment promoted by the ET_A receptor. Kinetics of activation of the indicated pathways following stimulation with vehicle or Endothelin-1 in HEK293 cells expressing the ET_A receptor. Data are means ± SD of two replicates of a representative experiment from three independent experiments and are expressed in % of the respective basal response (determined before ligand addition at t=0 sec).

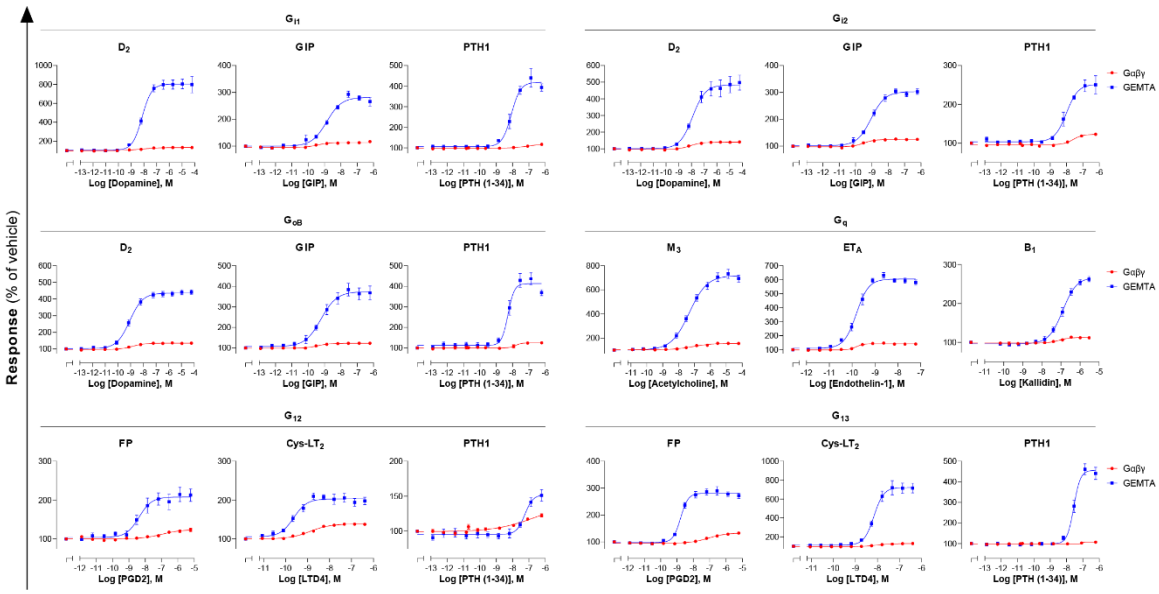

Figure S5. Comparison of EMTA platform and G protein activation BRET assay based on Gαβγ dissociation. Dose-response curves elicited in HEK293 cells transfected with the indicated receptor (D_2, GIP, PTH1, M_3, ET_A, B_1, FP or Cys-LT_2) and one of the $G\alpha_{i/o}$, $G\alpha_{q/11}$ or $G\alpha_{12/13}$ EMTA activation sensors, along with the indicated Gα subunits, or the BRET-based Gαβγ dissociation sensors (Gα-RlucII and GFP10-$G\gamma_1$ for $G\alpha_q$, $G\alpha_{12}$ and $G\alpha_{13}$ or GFP10-$G\gamma_2$ for $G\alpha_{i1}$, $G\alpha_{i2}$ and $G\alpha_{oB}$, with untagged $G\beta_1$). Data are means ± SEM from 3-7 independent experiments performed in one replicate and results are expressed in % of the response obtained for cells treated with vehicle.

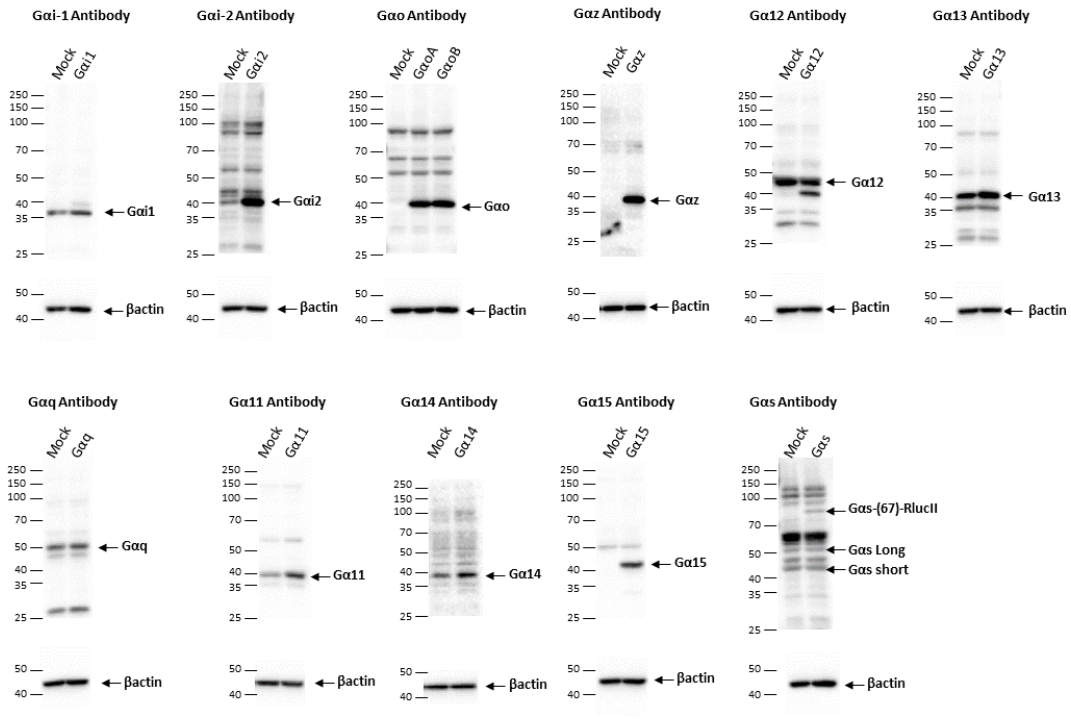

Figure S6. Western blot of G protein level expression in cells transfected with the EMTA ebBRET platform. G protein expression level detection in HEK293 cells transfected with the $G\alpha_{i/o}$, $G\alpha_{12/13}$, $G\alpha_{q/11}$ or $G\alpha_{s}$ activation sensors along with the indicated Gα protein or control DNA (Mock). Representative immunoblots of 3 independent experiments are shown.

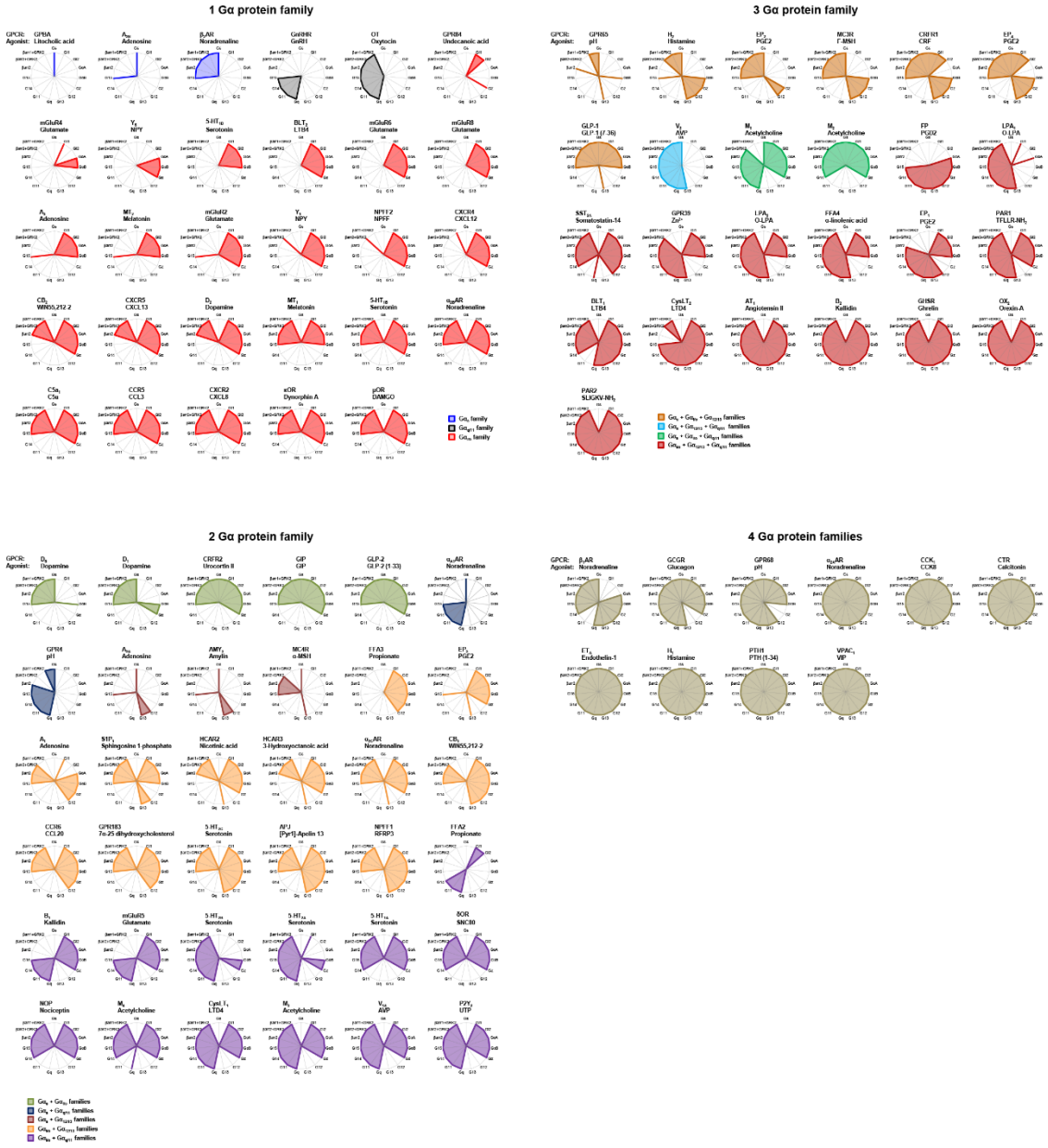

Figure S7. Receptor-specific signaling signatures. E_{max} values derived from concentration-response curves generated on 100 receptors using the 15 ebBRET-based assay are represented as radial graphs. A score of 0 indicates no coupling to a given pathway, whereas a score of 1 indicates a coupling. Receptors are rearranged according to the number of G protein families activated. $G\alpha_{15}$ has been considered apart from the $G_{q/11}$ family due to its promiscuous nature. See **Supplementary File 1** that shows the dose-response curves of the 100 receptors for the 15 different pathways.

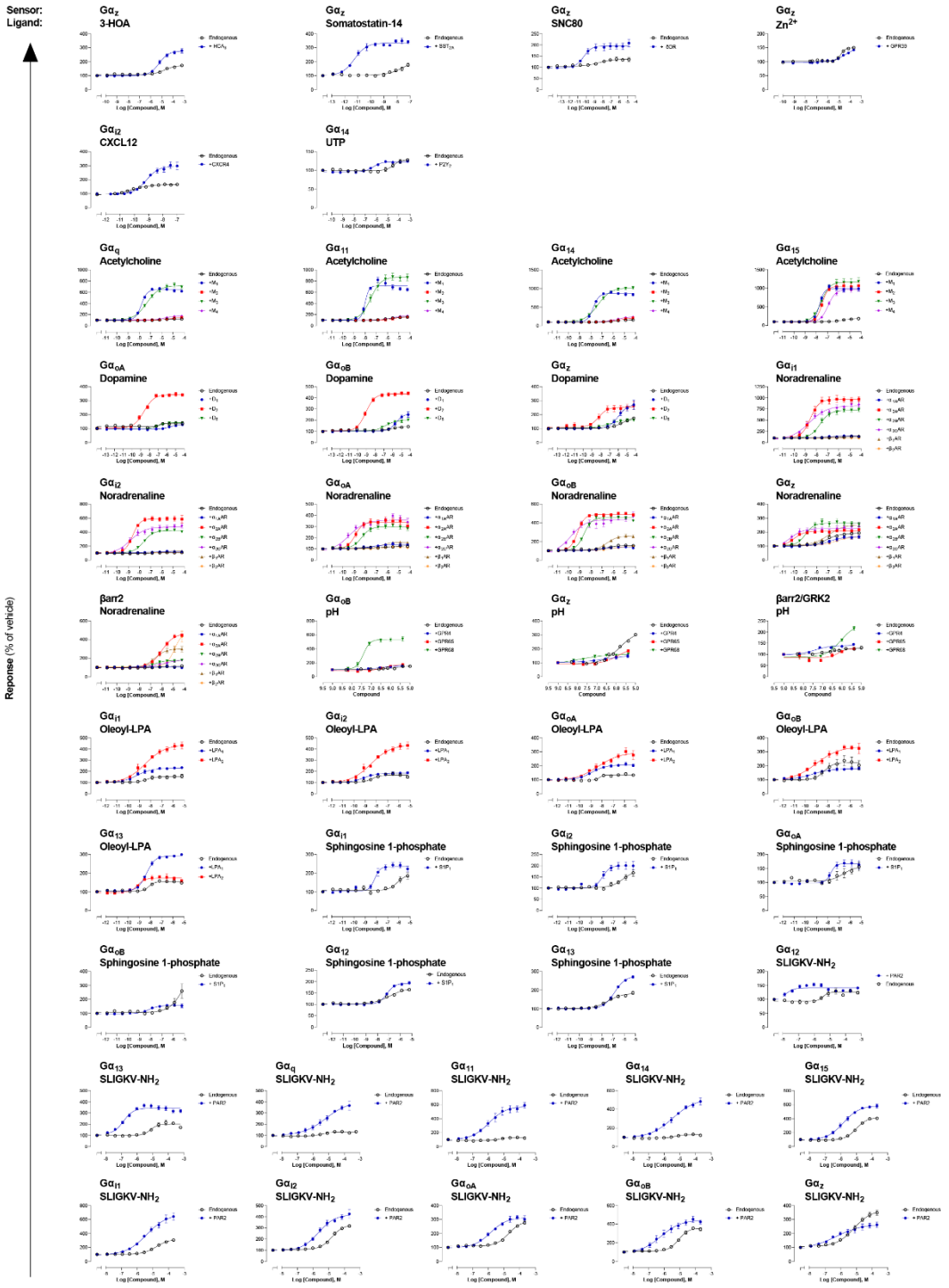

Figure S8. Detection of endogenous receptor-mediated responses with the EMTA ebBRET platform in HEK293 cells. Comparison of concentration-response curves elicited by the indicated ligand for a specific pathway, following the stimulation of HEK293 cells expressing endogenous or heterologously expressed receptors. The data presented refer to the ligands where a signal was detected on non-transfected cells (endogenous expression) (See **Supplementary File 1** for the curves on light gray and yellow background). Data are the mean ± SEM of at least 3 independent experiments performed in one replicate and expressed in % of the response obtained for cells treated with vehicle.

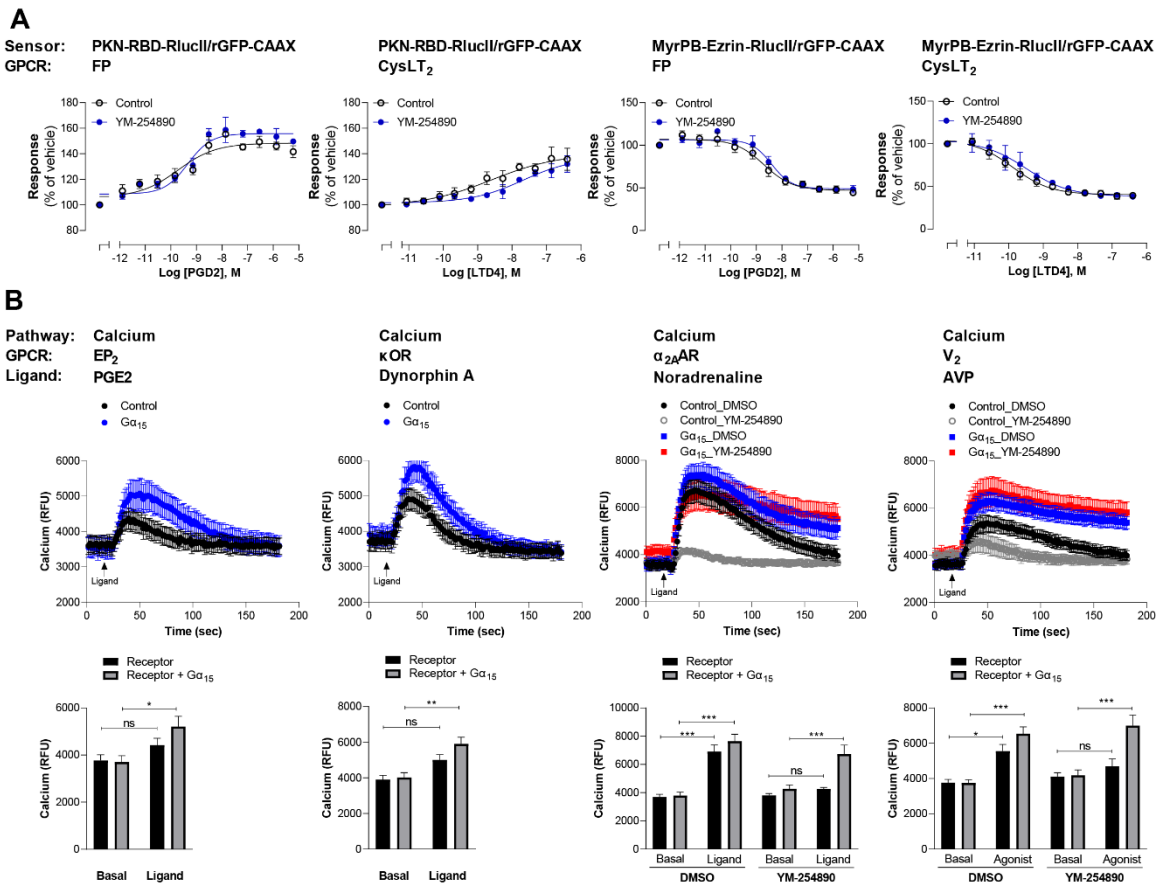

Figure S9. Validation of $G_{12/13}$ and G_{15} signaling for the newly characterized GPCRs. (**A**) Validation of $G_{12/13}$-mediated signal using Rho and Ezrin activation sensors. HEK293 cells expressing FP or $CysLT_2$ receptors and the PKN-RBD-RlucII or MyrPB-Ezrin-RlucII/rGFP-CAAX sensors were pretreated or not with the $G\alpha_q$ inhibitor YM-254890 and then stimulated with increasing concentrations of respective ligand. Data are means ± SEM from 3-5 independent experiments performed in one replicate and expressed in % of vehicle treated cells. (**B**) Validation of $G\alpha_{15}$-mediated signal by measuring calcium production. *Top*: Kinetics of calcium release induced by the indicated ligand in HEK293 cells expressing the indicated receptor, alone or with $G\alpha_{15}$ subunit. For receptors that also couple to other $G_{q/11}$ family members, cells were pretreated with DMSO or the $G\alpha_q$ inhibitor YM-254890. *Bottom*: The peak of calcium production obtained from kinetics were compared to the basal level of calcium (determined between 0 and 17 sec). Data are means ± SEM from 5-7 independent experiments performed in one replicate and expressed in relative fluorescence unit (RFU). Two Way ANOVA test: *$p < 0.05$, **$p < 0.01$ and ***$p < 0.001$ compared to respective basal calcium level. ns: not significant.

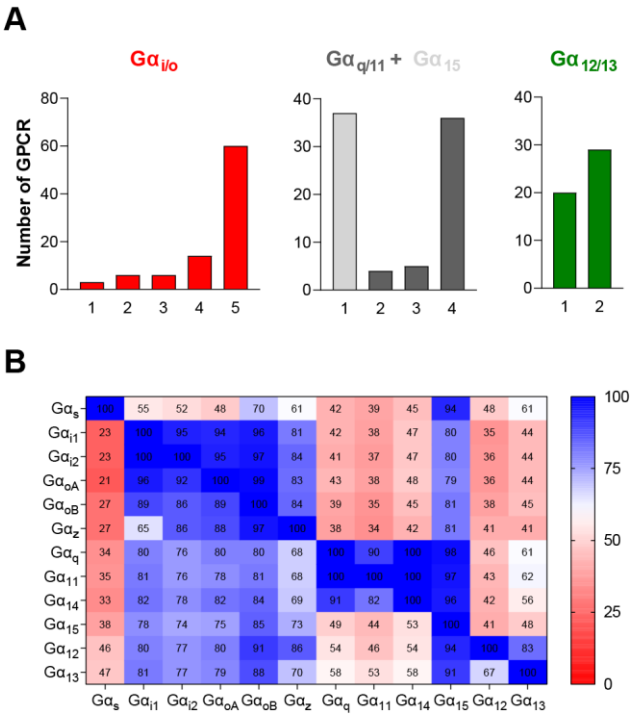

Figure S10. G protein subtypes distribution across the 100 GPCRs profiled with the EMTA ebBRET-based platform. (**A**) Number of receptors that can couple to 1 to 5 of the different subtypes from each G protein family. (**B**) % of receptors activating a specific G protein subtype (Y axis) that also activate another G protein subtype (X axis).

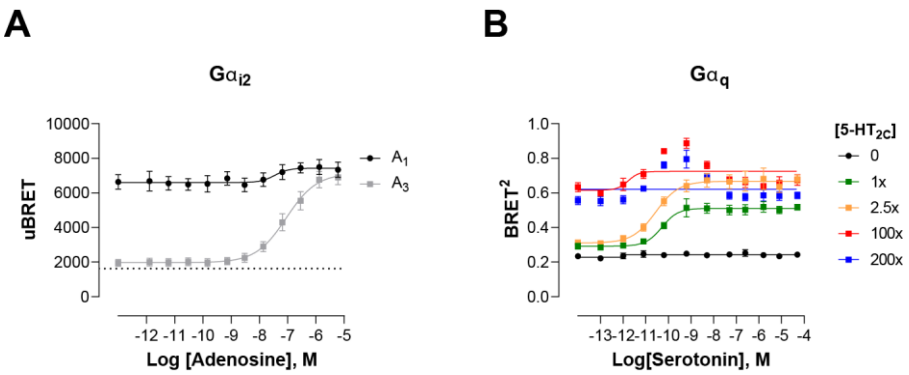

Figure S11. Modulation of ligand-promoted response detected by EMTA ebBRET platform by receptor constitutive activity. (**A**) Concentration-response curves of $G\alpha_{i2}$ activation elicited by adenosine in HEK293 cells transfected with the Rap1GAP-RlucII/rGFP-CAAX sensors with untagged $G\alpha_{i2}$ and A_1 or A_3 receptors. Basal level of G_{i2} activation detected by the GEMTA sensor in absence of heterologous receptor expression is represented by the interrupted line. Data are expressed as uBRET ratio and are means ± SEM of 4 independent experiments performed in one replicate. (**B**) Concentration-response curves of $G\alpha_q$ activation elicited by serotonin in HEK293 cells transfected with the p63-RlucII/rGFP-CAAX sensors with untagged $G\alpha_q$ and increasing amount of 5-HT_{2C} receptor plasmid. Data are expressed as BRET ratio and are means ± SEM of 4 independent experiments performed in one replicate.

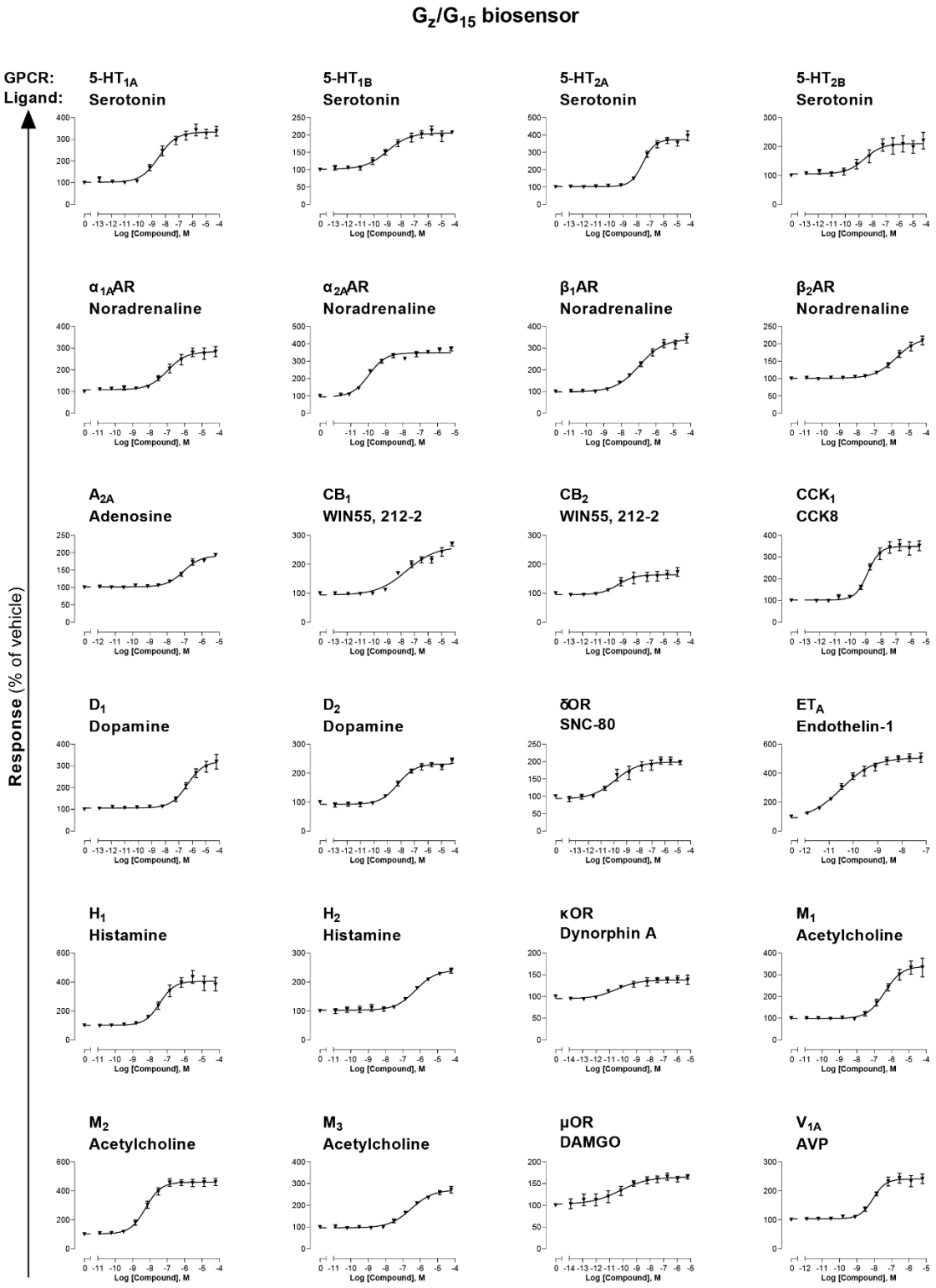

Figure S12. Combined G_z/G_{15} biosensor. HEK293 cells transfected with the Rap1GAP-RlucII/p63-RhoGEF-RlucII/rGFP-CAAX sensors along with $G\alpha_z$ and $G\alpha_{15}$ subunits and the indicated untagged receptor were stimulated with increasing concentrations of the indicated ligand. Data are means ± SEM from 3-5 independent experiments performed in one replicate and results are expressed in % of vehicle treated cells.

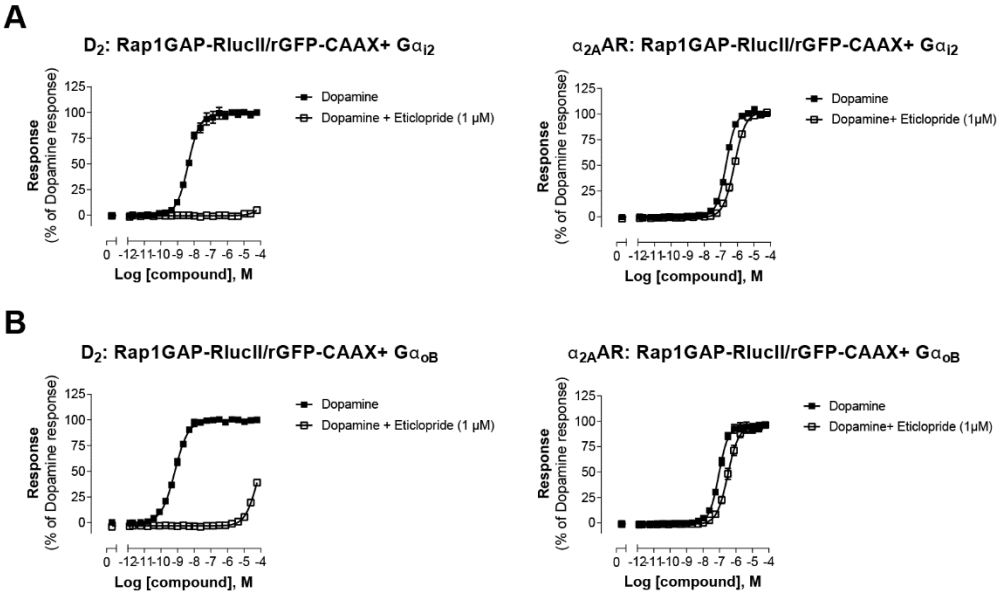

Figure S13. Validation of direct activation of α_{2A}AR by Dopamine. HEK293 cells expressing D_2 or α_{2A}AR and the $G\alpha_{i2}$ (**A**) or the $G\alpha_{oB}$ (**B**) sensors were pretreated or not with the selective D_2-family antagonist eticlopride, before stimulation with increasing concentrations of dopamine. Data are means ± SEM from 2-4 independent experiments performed in one replicate and expressed in % of the response elicited by dopamine.

Supplementary Materials

Supplementary File 1. Signaling profiles of 100 therapeutically-relevant human GPCRs using the EMTA ebBRET platform. Concentration-response curves in HEK293 cells expressing the indicated biosensor after stimulation of heterologously expressed receptor with the indicated ligand. Data are means ± SEM from at least 3 independent experiments and expressed in % of the response obtained for cells treated with vehicle. For ligands that elicited endogenous receptor-mediated responses (curves with light gray and yellow background for responses similar to and better responses than those obtained with the endogenous receptors, respectively), curves from cells expressing endogenous or heterologously expressed receptors are shown in **Figure S8**.

Supplementary Table 1. (**A**) **Absolute pEC_{50} values of responses elicited in WT *vs.* Knockout Gα protein background cells.** pEC_{50} values deduced from dose-response curves for various receptor tested in parental (WT) HEK293 cells or devoid of G_s, $G_{12/13}$, $G_{q/11}$ or $G_{i/o}$ proteins are related to **Figure S1**. (**B**) **Absolute pEC_{50} values of responses elicited in cells transfected with different amounts of Gα proteins.** pEC_{50} values deduced from dose-response curves obtained following Gα subunit titration in HEK293 cells transfected with GEMTA sensors and related to **Figure S3A**. (**C**) **Absolute pEC_{50} values of responses elicited in cells transfected with different amounts of receptors.** pEC_{50} values deduced from dose-response curves obtained following ET_A titration in HEK293 cells transfected with GEMTA sensors and related to **Figure S3B.** (**D**) **Absolute pEC_{50} values of responses elicited in cells transfected with different amounts of Effector-RlucII**. pEC_{50} values

deduced from dose-response curves obtained following Effector-RlucII titration in HEK293 cells transfected with GEMTA sensors and related to **Figure S3C**.

Supplementary Table 2. List of tested receptors and ligands, along with the raw E_{max}, absolute pEC_{50} and their corresponding double normalized (dnor) values. The E_{max} (in % of vehicle response) and absolute pEC_{50} values deduced from concentration-response curves for the 100 GPCRs tested as well as the double normalized E_{max} and pEC_{50} values calculated are related to **Supplementary File 1** and **Figure 3**, respectively.

Supplementary Table 3. Comparison of G protein couplings identified with EMTA platform and other datasets. Comparison of G protein couplings identified with EMTA platform and TGF-α shedding assay in Inoue *et al.*, 2019 (**A**) or reported in GtP database (**B**).

Video 1. BRET-based imagery of p63-RhoGEF-RlucII recruitment to plasma membrane upon GnRHR activation. HEK293 cells expressing the p63-RhoGEF-RlucII/rGFP-CAAX sensors with $G\alpha_q$ and GnRHR were stimulated with GnRH. BRET levels (the ratio of the acceptor photon count to the total photon count) are expressed as a color code (lowest being black and purple, and highest being red and white).

Video 2. BRET-based imagery of Rap1GAP-RlucII recruitment to plasma membrane upon D_2 activation. HEK293 cells expressing the Rap1GAP-RlucII/rGFP-CAAX sensors with $G\alpha_{i2}$ and D_2 were stimulated with dopamine. BRET levels (the ratio of the acceptor photon

count to the total photon count) are expressed as a color code (lowest being black and purple, and highest being red and white).

Video 3. BRET-based imagery of PDZ-RhoGEF-RlucII recruitment to plasma membrane upon TPαR activation. HEK293 cells expressing the PDZ-RhoGEF-RlucII/rGFP-CAAX + $G\alpha_{13}$ and TPαR were stimulated with U46619. BRET levels (the ratio of the acceptor photon count to the total photon count) are expressed as a color code (lowest being black and purple, and highest being red and white).

Since videos cannot be accepted on the bioRvix site, we have generated figures that show the first and last image of each video that have been submitted to the journal (see below).

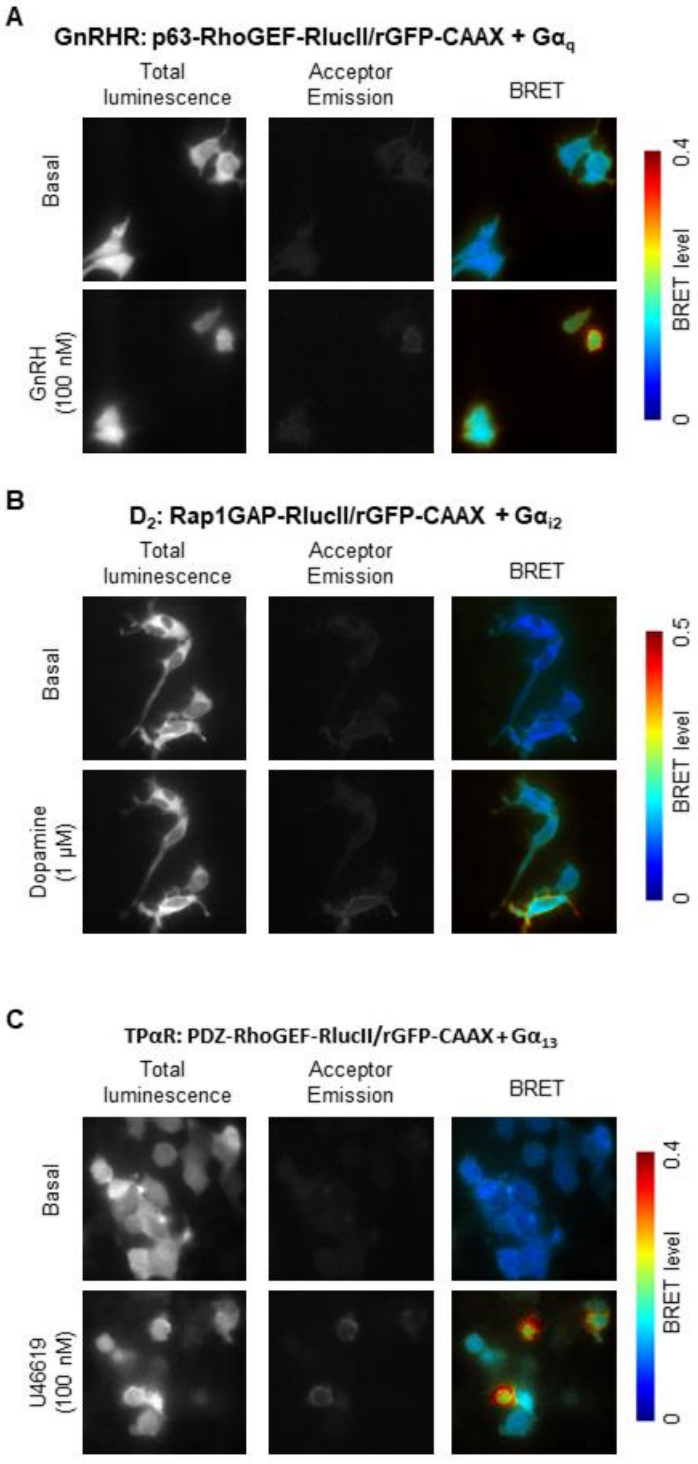

BRET-based imagery showing sensor recruitment to the plasma membrane upon receptor activation, using the effector membrane translocation assay (EMTA).

(**A**) p63-RhoGEF-RlucII recruitment to plasma membrane upon GnRHR activation. HEK293 cells expressing the p63-RhoGEF-RlucII/rGFP-CAAX sensors with $G\alpha_q$ and GnRHR were stimulated with 100 nM GnRH.

(**B**) Rap1GAP-RlucII recruitment to plasma membrane upon D_2 activation. HEK293 cells expressing the Rap1GAP-RlucII/rGFP-CAAX sensors with $G\alpha_{i2}$ and D_2 were stimulated with 1 µM dopamine.

(**C**) PDZ-RhoGEF-RlucII recruitment to plasma membrane upon TPαR activation. HEK293 cells expressing the PDZ-RhoGEF-RlucII/rGFP-CAAX + $G\alpha_{13}$ and TPαR were stimulated with 100 nM U46619.

Images were obtained in basal condition and 200 sec after stimulation with agonist. In each image, BRET levels (the ratio of the acceptor photon count to the total photon count) are expressed as a heat map color code (lowest being black and purple, and highest being red and white), as shown in the right of the panel.